CHAPTER

8

GUIDED-WAVE OPTICS

John Tyndall (1820–1893) was the first to demonstrate total internal reflection, the basis of guided-wave optics.

In traditional optical instruments and systems, light is transmitted between different locations in the form of beams that are collimated, relayed, focused, and scanned by mirrors, lenses, and prisms. The beams diffract and broaden as they propagate though they can be refocused by the use of lenses and mirrors. However, the bulk optical components that comprise such systems are often large and unwieldy, and objects in the paths of the beams can obstruct or scatter them.

In many circumstances it is advantageous to transmit optical beams through dielectric conduits rather than through free space. The technology for achieving this is known as **guided-wave optics**. It was initially developed to provide long-distance light transmission without the necessity of using relay lenses. This technology now has many important applications. A few examples are: carrying light over long distances for lightwave communications, biomedical imaging where light must reach awkward locations, and connecting components within miniaturized optical and optoelectronic devices and systems.

The underlying principle of optical confinement is simple. A medium of refractive index n_1, embedded in a medium of lower refractive index $n_2 < n_1$, acts as a light "trap" within which optical rays remain confined by multiple total internal reflections at the boundaries. Because this effect facilitates the confinement of light generated inside a medium of high refractive index [see Exercise (1.2-6)], it can be exploited in making light conduits — guides that transport light from one location to another. An **optical waveguide** is a light conduit consisting of a slab, strip, or cylinder of dielectric material embedded in another dielectric material of lower refractive index (Fig. 8.0-1). The light is transported through the inner medium without radiating into the surrounding medium. The most widely used of these waveguides is the optical fiber, comprising two concentric cylinders of low-loss dielectric material such as glass (see Chapter 9).

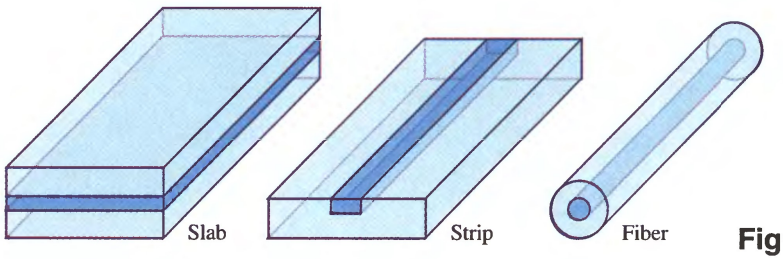

Figure 8.0-1 Optical waveguides.

Integrated optics is the technology of combining, on a single substrate ("chip"), various optical devices and components useful for generating, focusing, splitting, combining, isolating, polarizing, coupling, switching, modulating, and detecting light. Optical waveguides provide the links among these components. Such chips (Fig. 8.0-2) are optical versions of electronic integrated circuits. Integrated optics has, as its goal, the miniaturization of optics in much the same way that integrated circuits have served to miniaturize electronics.

This Chapter

The basic theory of optical waveguides is presented in this and the following chapter. In this chapter, we consider rectangular waveguides, which are used extensively in integrated optics. Chapter 9 deals with cylindrical waveguides, i.e., optical fibers. If reflectors are placed at the two ends of a short waveguide, the result is a structure that traps and stores light – an optical resonator. These devices, which are essential to lasers, are described in Chapter 10. Other integrated-optic components and devices (such as semiconductor lasers, detectors, modulators, and switches) are considered in

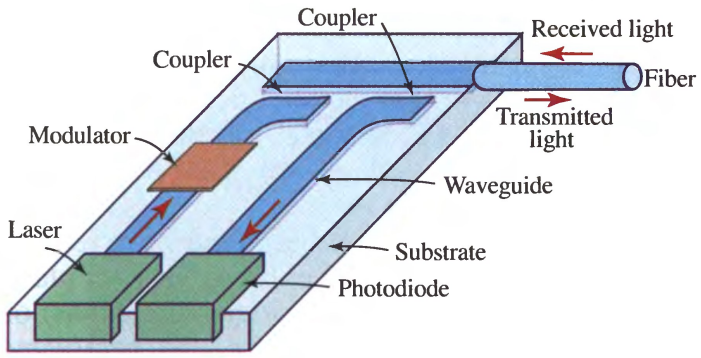

Figure 8.0-2 Example of an integrated-optic device used as an optical receiver/transmitter. Received light is coupled into a waveguide and directed to a photodiode where it is detected. Light from a laser is guided, modulated, and coupled into a fiber for transmission.

the chapters that deal specifically with those components and devices. Optical fiber communication systems are discussed in detail in Chapter 24.

8.1 PLANAR-MIRROR WAVEGUIDES

We begin by examining wave propagation in a waveguide comprising two parallel infinite planar *mirrors* separated by a distance d (Fig. 8.1-1). The mirrors are assumed to reflect light without loss. A ray of light, say in the y–z plane, making an angle θ with the mirrors reflects and bounces between them without loss of energy. The ray is thus guided along the z direction.

This waveguide appears to provide a perfect conduit for light rays. It is *not* used in practical applications, however, principally because of the difficulty and cost of fabricating low-loss mirrors. Nevertheless, we study this simple example in detail because it provides a valuable pedagogical introduction to the dielectric waveguide, which we examine in Sec. 8.2, and to the optical resonator, which is the subject of Chapter 10.

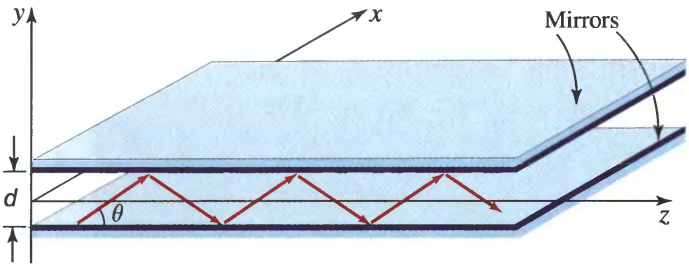

Figure 8.1-1 Planar-mirror waveguide.

Waveguide Modes

The ray-optics picture of light being guided by multiple reflections cannot explain a number of important effects that require the use of electromagnetic theory. A simple approach for carrying out an electromagnetic analysis is to associate with each optical ray a transverse electromagnetic (TEM) plane wave. The total electromagnetic field is then the sum of these plane waves.

Consider a monochromatic TEM plane wave of wavelength $\lambda = \lambda_o/n$, wavenumber $k = nk_o$, and phase velocity $c = c_o/n$, where n is the refractive index of the medium between the mirrors. The wave is polarized in the x direction and its wavevector lies in the y–z plane at an angle θ with the z axis (Fig. 8.1-1). Like the optical ray, the wave reflects from the upper mirror, travels at an angle $-\theta$, reflects from the lower mirror, and travels once more at an angle θ, and so on. Since the electric-field vector is parallel

to the mirror, each reflection is accompanied by a phase shift π for a perfect mirror, but the amplitude and polarization are not changed. The π phase shift ensures that the sum of each wave and its own reflection vanishes so that the total field is zero at the mirrors. At each point within the waveguide we have TEM waves traveling upward at an angle θ and others traveling downward at an angle $-\theta$; all waves are polarized in the x direction.

We now impose a self-consistency condition by requiring that as the wave reflects twice, it reproduces itself [see Fig. 8.1-2(a)], so that we have only two distinct plane waves. Fields that satisfy this condition are called the modes (or eigenfunctions) of the waveguide (see Appendix C). *Modes are fields that maintain the same transverse distribution and polarization at all locations along the waveguide axis.* We shall see that self-consistency guarantees this shape invariance. In connection with Fig. 8.1-2, the phase shift $\Delta\varphi$ encountered by the original wave in traveling from A to B must be equal to, or differ by an integer multiple of 2π, from that encountered when the wave reflects, travels from A to C, and reflects once more. Accounting for a phase shift of π at each reflection, we have $\Delta\varphi = 2\pi\overline{AC}/\lambda - 2\pi - 2\pi\overline{AB}/\lambda = 2\pi q$, where $q = 0, 1, 2, \ldots$, so that $2\pi(\overline{AC} - \overline{AB})/\lambda = 2\pi(q+1)$. The geometry portrayed in Fig. 8.1-2(a), together with the identity $\cos(2x) = 1 - 2\sin^2 x$, provides $\overline{AC} - \overline{AB} = 2d\sin\theta$, where d is the distance between the mirrors. Thus, $2\pi(2d\sin\theta)/\lambda = 2\pi(q+1)$ so that

$$\frac{2\pi}{\lambda}\, 2d\, \sin\theta = 2\pi\, m, \qquad m = 1, 2, \ldots. \tag{8.1-1}$$

where $m = q + 1$. The self-consistency condition is therefore satisfied only for certain bounce angles $\theta = \theta_m$ satisfying

$$\boxed{\sin\theta_m = m\,\frac{\lambda}{2d}, \qquad m = 1, 2, \ldots.} \tag{8.1-2}$$

Bounce Angles

Each integer m corresponds to a bounce angle θ_m, and the corresponding field is called the mth mode. The $m = 1$ mode has the smallest angle, $\theta_1 = \sin^{-1}(\lambda/2d)$; modes with larger m are composed of more oblique plane-wave components.

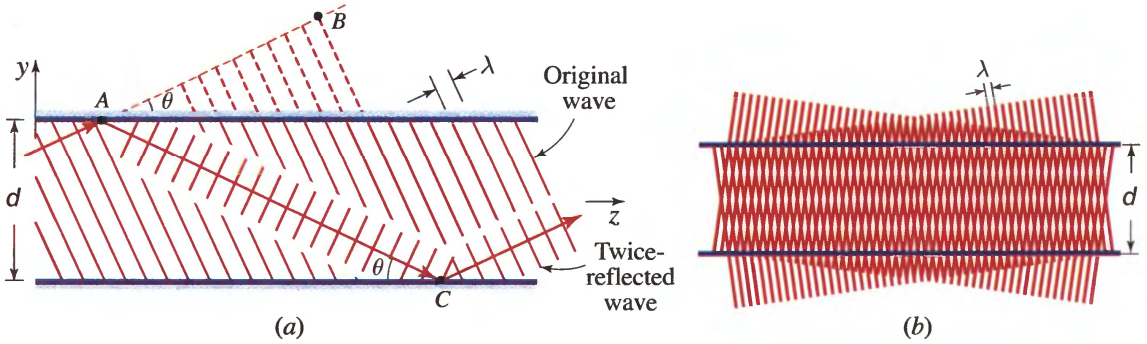

Figure 8.1-2 (a) Condition of self-consistency: as a wave reflects twice it duplicates itself. (b) At angles for which self-consistency is satisfied, the two waves interfere and create a pattern that does not change with z.

When the self-consistency condition is satisfied, the phases of the upward and downward plane waves at points on the z axis differ by half the round-trip phase shift $q\pi$,

$q = 0, 1, \ldots$, or $(m-1)\pi$, $m = 1, 2, \ldots$, so that they add for odd m and subtract for even m.

Since the y component of the propagation constant is given by $k_y = nk_o \sin\theta$, it is quantized to the values $k_{ym} = nk_o \sin\theta_m = (2\pi/\lambda)\sin\theta_m$. Using (8.1-2), we obtain

$$\boxed{k_{ym} = m\frac{\pi}{d},} \qquad m = 1, 2, 3 \ldots, \tag{8.1-3}$$

Wavevector Transverse Component

so that the k_{ym} are spaced by π/d. Equation (8.1-3) states that the phase shift encountered when a wave travels a distance $2d$ (one round trip) in the y direction, with propagation constant k_{ym}, must be a multiple of 2π.

Propagation Constants

A guided wave is composed of two distinct plane waves traveling in the y–z plane at angles $\pm\theta$ with the z axis. Their wavevectors have components $(0, k_y, k_z)$ and $(0, -k_y, k_z)$. Their sum or difference therefore varies with z as $\exp(-jk_z z)$, so that the propagation constant of the guided wave is $\beta \equiv k_z = k\cos\theta$. Thus, β is quantized to the values $\beta_m = k\cos\theta_m$, from which $\beta_m^2 = k^2(1 - \sin^2\theta_m)$. Using (8.1-2), we obtain

$$\boxed{\beta_m^2 = k^2 - \frac{m^2\pi^2}{d^2}.} \tag{8.1-4}$$

Propagation Constants

Higher-order (more oblique) modes travel with smaller propagation constants. The values of θ_m, k_{ym}, and β_m for the different modes are illustrated in Fig. 8.1-3.

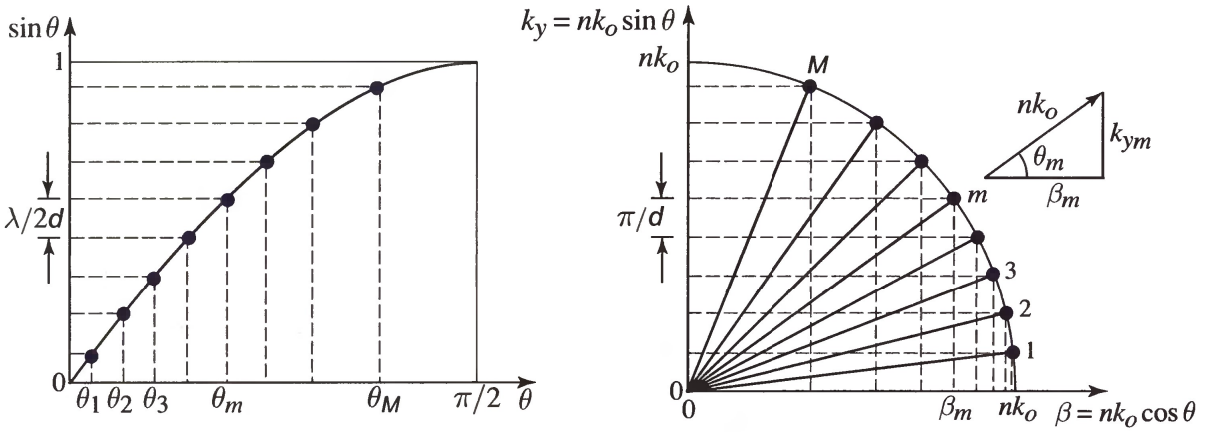

Figure 8.1-3 The bounce angles θ_m and the wavevector components of the modes of a planar-mirror waveguide (indicated by dots). The transverse components $k_{ym} = k\sin\theta_m$ are spaced uniformly at multiples of π/d, but the bounce angles θ_m and the propagation constants β_m are not equally spaced. Mode $m = 1$ has the smallest bounce angle and the largest propagation constant.

Field Distributions

The complex amplitude of the total field in the waveguide is the superposition of the two bouncing TEM plane waves. If $A_m \exp(-jk_{ym}y - j\beta_m z)$ is the upward wave, then $e^{j(m-1)\pi} A_m \exp(+jk_{ym}y - j\beta_m z)$ must be the downward wave [at $y = 0$, the two waves differ by a phase shift $(m-1)\pi$]. There are therefore symmetric modes, for which the two plane-wave components are added, and antisymmetric modes, for which they are subtracted. The total field turns out to be $E_x(y,z) = 2A_m \cos(k_{ym}y)\exp(-j\beta_m z)$ for odd modes and $2jA_m \sin(k_{ym}y)\exp(-j\beta_m z)$ for even modes.

Using (8.1-3) we write the complex amplitude of the electric field in the form

$$E_x(y,z) = \mathcal{a}_m u_m(y)\exp(-j\beta_m z), \tag{8.1-5}$$

where

$$u_m(y) = \begin{cases} \sqrt{\dfrac{2}{d}}\cos\left(m\pi\dfrac{y}{d}\right), & m = 1,3,5,\ldots \\ \sqrt{\dfrac{2}{d}}\sin\left(m\pi\dfrac{y}{d}\right), & m = 2,4,6,\ldots, \end{cases} \tag{8.1-6}$$

with $\mathcal{a}_m = \sqrt{2d}\,A_m$ and $j\sqrt{2d}\,A_m$, for odd m and even m, respectively. The functions $u_m(y)$ have been normalized to satisfy

$$\int_{-d/2}^{d/2} u_m^2(y)\,dy = 1. \tag{8.1-7}$$

Thus, $\mathcal{a}_m$ is the amplitude of mode m. It can be shown that the functions $u_m(y)$ also satisfy

$$\int_{-d/2}^{d/2} u_m(y)\,u_l(y)\,dy = 0, \qquad l \neq m, \tag{8.1-8}$$

i.e., they are orthogonal in the $[-d/2, d/2]$ interval.

The transverse distributions $u_m(y)$ are plotted in Fig. 8.1-4. Each mode can be viewed as a standing wave in the y direction, traveling in the z direction. Modes of large m vary in the transverse plane at a greater rate k_y and travel with a smaller propagation constant β. The field vanishes at $y = \pm d/2$ for all modes, so that the boundary conditions at the surface of the mirrors are always satisfied.

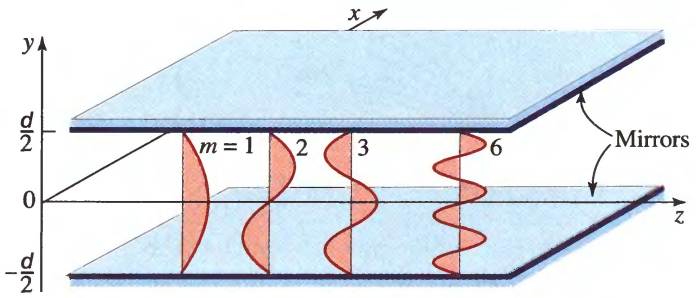

Figure 8.1-4 Field distributions of the modes of a planar-mirror waveguide.

Since we assumed at the outset that the bouncing TEM plane wave is polarized in the x direction, the total electric field is also in the x direction and the guided wave is a transverse-electric (TE) wave. Transverse magnetic (TM) waves are analyzed in a similar fashion as will be seen subsequently.

EXERCISE 8.1-1

Optical Power. Show that the optical power flow in the z direction associated with the TE mode $E_x(y,z) = \mathcal{A}_m u_m(y) \exp(-j\beta_m z)$ is $(|\mathcal{A}_m|^2/2\eta)\cos\theta_m$, where $\eta = \eta_o/n$ and $\eta_o = \sqrt{\mu_o/\epsilon_o}$ is the impedance of free space.

Number of Modes

Since $\sin\theta_m = m\lambda/2d$, $m = 1, 2, \ldots$, and taking $\sin\theta_m < 1$, the maximum allowed value of m is the greatest integer smaller than $1/(\lambda/2d)$,

$$M \doteq \frac{2d}{\lambda}. \tag{8.1-9}$$

Number of Modes

The symbol $\doteq$ denotes that $2d/\lambda$ is reduced to the nearest integer. As examples, when $2d/\lambda = 0.9$, 1, and 1.1, we have $M = 0$, 0, and 1, respectively. Thus, M is the number of modes of the waveguide. Light can be transmitted through the waveguide in one, two, or many modes. The actual number of modes that carry optical power depends on the source of excitation, but the maximum number is M.

The number of modes increases with increasing ratio of the mirror separation to the wavelength. Under conditions such that $2d/\lambda \leq 1$, corresponding to $d \leq \lambda/2$, M is seen to be 0, which indicates that the self-consistency condition cannot be met and the waveguide cannot support any modes. The wavelength $\lambda_c = 2d$ is called the **cutoff wavelength** of the waveguide. It is the longest wavelength that can be guided by the structure. It corresponds to the **cutoff frequency**

$$\nu_c = \frac{c}{2d}, \tag{8.1-10}$$

Cutoff Frequency

or the cutoff angular frequency $\omega_c = 2\pi\nu_c = \pi c/d$, the lowest frequency of light that can be guided by the waveguide. If $1 < 2d/\lambda \leq 2$ (i.e., $d \leq \lambda < 2d$ or $\nu_c \leq \nu < 2\nu_c$), only one mode is allowed. The structure is then said to be a **single-mode waveguide**. If $d = 5$ μm, for example, the waveguide has a cutoff wavelength $\lambda_c = 10$ μm; it supports a single mode for 5 μm $\leq \lambda < 10$ μm, and more modes for $\lambda < 5$ μm. Equation (8.1-9) can also be written in terms of the frequency ν, $M \doteq \nu/\nu_c = \omega/\omega_c$, so that the number of modes increases by unity when the angular frequency ω is incremented by ω_c, as illustrated in Fig. 8.1-5(a).

Dispersion Relation

The relation between the propagation constant β and the angular frequency ω is an important characteristic of the waveguide, known as the **dispersion relation**. For a homogeneous medium, the dispersion relation is simply $\omega = c\beta$. For mode m of a planar-mirror waveguide, β_m and ω are related by (8.1-4) so that

$$\beta_m^2 = (\omega/c)^2 - m^2\pi^2/d^2. \tag{8.1-11}$$

This relation may be written in terms of the cutoff angular frequency $\omega_c = 2\pi\nu_c = \pi c/d$ as

$$\beta_m = \frac{\omega}{c}\sqrt{1 - m^2\frac{\omega_c^2}{\omega^2}}\,. \tag{8.1-12}$$

Dispersion Relation

As shown in Fig. 8.1-5(b) for $m = 1, 2, \ldots$, the propagation constant β for mode m is zero at angular frequency $\omega = m\omega_c$, increases monotonically with angular frequency, and ultimately approaches the linear relation $\beta = \omega/c$ for sufficiently large values of β.

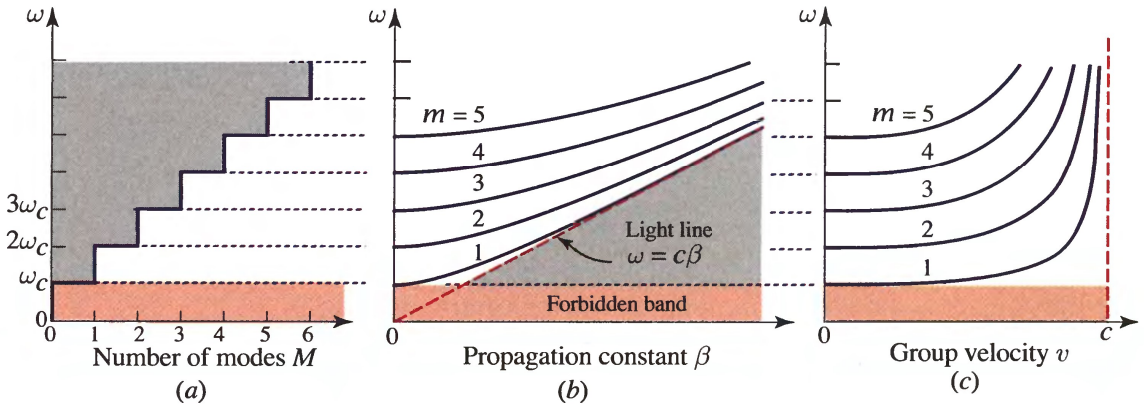

Figure 8.1-5 (a) Number of modes M as a function of angular frequency ω. Modes are not permitted for angular frequencies below the cutoff, $\omega_c = \pi c/d$. M increments by unity as ω increases by ω_c. (b) Dispersion relation. A forbidden band exists for angular frequencies below ω_c. (c) Group velocities of the modes as a function of angular frequency.

Group Velocities

In a medium with a given ω-β dispersion relation, a pulse of light (wavepacket) that has an angular frequency centered at ω travels with a velocity $v = d\omega/d\beta$, known as the group velocity (see Sec. 5.6). Taking the derivative of (8.1-12) and assuming that c is independent of ω (i.e., ignoring dispersion in the waveguide material), we obtain $2\beta_m\, d\beta_m/d\omega = 2\omega/c^2$, so that $d\omega/d\beta_m = c^2\beta_m/\omega = c^2 k\cos\theta_m/\omega = c\cos\theta_m$, from which the group velocity of mode m is

$$v_m = c\cos\theta_m = c\sqrt{1 - m^2\frac{\omega_c^2}{\omega^2}}\,. \tag{8.1-13}$$

Group Velocity

It follows that more oblique modes travel with smaller group velocities since they are delayed by the longer paths of the zigzagging process. The dependence of the group velocity on angular frequency is illustrated in Fig. 8.1-5(c), which shows that for each mode, the group velocity increases monotonically from 0 to c as the angular frequency increases above the mode cutoff frequency.

Equation (8.1-13) may also be obtained geometrically by examining the plane wave as it bounces between the mirrors and determining the distance advanced in the z

direction and the time taken by the zigzagging process. For the trip from the bottom mirror to the top mirror (Fig. 8.1-6) we have

$$v = \frac{\text{distance}}{\text{time}} = \frac{d\cot\theta}{d\csc\theta/c} = c\cos\theta. \tag{8.1-14}$$

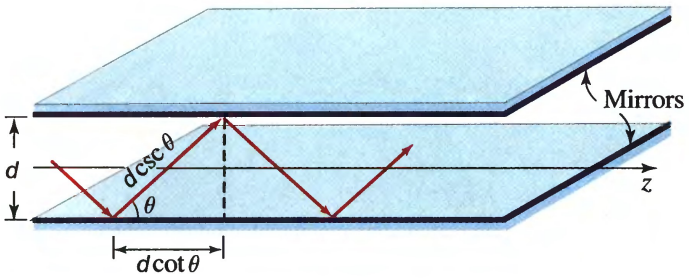

Figure 8.1-6 A plane wave bouncing at an angle θ advances in the z direction by a distance $d\cot\theta$ in a time $d\csc\theta/c$. The velocity is $c\cos\theta$.

TM Modes

Only TE modes (electric field in the x direction) have been considered to this point. TM modes (magnetic field in the x direction) can also be supported by the mirror waveguide. They can be studied by means of a TEM plane wave with the magnetic field in the x direction, traveling at an angle θ and reflecting from the two mirrors (Fig. 8.1-7). The electric-field complex amplitude then has components in the y and z directions. Since the z component is parallel to the mirror, it behaves precisely like the x component of the TE mode (i.e., it undergoes a phase shift π at each reflection and vanishes at the mirrors). When the self-consistency condition is applied to this component the result is mathematically identical to that of the TE case. The angles θ, the transverse wavevector components k_y, and the propagation constants β of the TM modes associated with this component are identical to those of the TE modes. There are $M \doteq 2d/\lambda$ TM modes (and a total of $2M$ modes) supported by the waveguide.

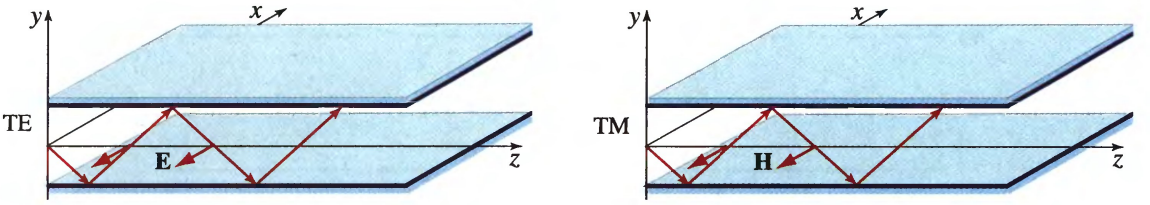

Figure 8.1-7 TE and TM polarized guided waves.

The z component of the electric-field complex amplitude of mode m, as previously, is the sum of an upward plane wave $A_m \exp(-jk_{ym}y)\exp(-j\beta_m z)$ and a downward plane wave $e^{j(m-1)\pi}A_m \exp(jk_{ym}y)\exp(-j\beta_m z)$, with equal amplitudes and phase shift $(m-1)\pi$, so that

$$E_z(y,z) = \begin{cases} a_m\sqrt{\dfrac{2}{d}}\cos\left(m\pi\dfrac{y}{d}\right)\exp(-j\beta_m z), & m = 1,3,5,\ldots \\ a_m\sqrt{\dfrac{2}{d}}\sin\left(m\pi\dfrac{y}{d}\right)\exp(-j\beta_m z), & m = 2,4,6,\ldots, \end{cases} \tag{8.1-15}$$

where $a_m = \sqrt{2d}\,A_m$ and $j\sqrt{2d}\,A_m$ for odd and even m, respectively. Since the electric-field vector of a TEM plane wave is normal to its direction of propagation, it

makes an angle $\pi/2 + \theta_m$ with the z axis for the upward wave, and $\pi/2 - \theta_m$ for the downward wave.

The y components of the electric field of these waves are

$$A_m \cot\theta_m \exp(-jk_{ym}y)\exp(-j\beta_m z) \text{ and } e^{jm\pi} A_m \cot\theta_m \exp(jk_{ym}y)\exp(-j\beta_m z), \tag{8.1-16}$$

so that

$$E_y(y,z) = \begin{cases} a_m\sqrt{\dfrac{2}{d}}\cot\theta_m \cos\left(m\pi\dfrac{y}{d}\right)\exp(-j\beta_m z), & m = 1,3,5,\ldots \\ a_m\sqrt{\dfrac{2}{d}}\cot\theta_m \sin\left(m\pi\dfrac{y}{d}\right)\exp(-j\beta_m z), & m = 2,4,6,\ldots. \end{cases} \tag{8.1-17}$$

Satisfaction of the boundary conditions is assured because $E_z(y,z)$ vanishes at the mirrors. The magnetic field component $H_x(y,z)$ may be similarly determined by noting that the ratio of the electric to the magnetic fields of a TEM wave is the impedance of the medium η. The resultant fields $E_y(y,z)$, $E_z(y,z)$, and $H_x(y,z)$ do, of course, satisfy Maxwell's equations.

Multimode Fields

For light to be guided by the mirrors, it is not necessary that it have the distribution of one of the modes. In fact, a field satisfying the boundary conditions (vanishing at the mirrors) but otherwise having an arbitrary distribution in the transverse plane *can* be guided by the waveguide. The optical power, however, is then divided among the modes. Since different modes travel with different propagation constants and different group velocities, the transverse distribution of the field will alter as it travels through the waveguide. Fig. 8.1-8 illustrates how the transverse distribution of a single mode is invariant to propagation, whereas the multimode distribution varies with z (the illustration is for the *intensity* distribution).

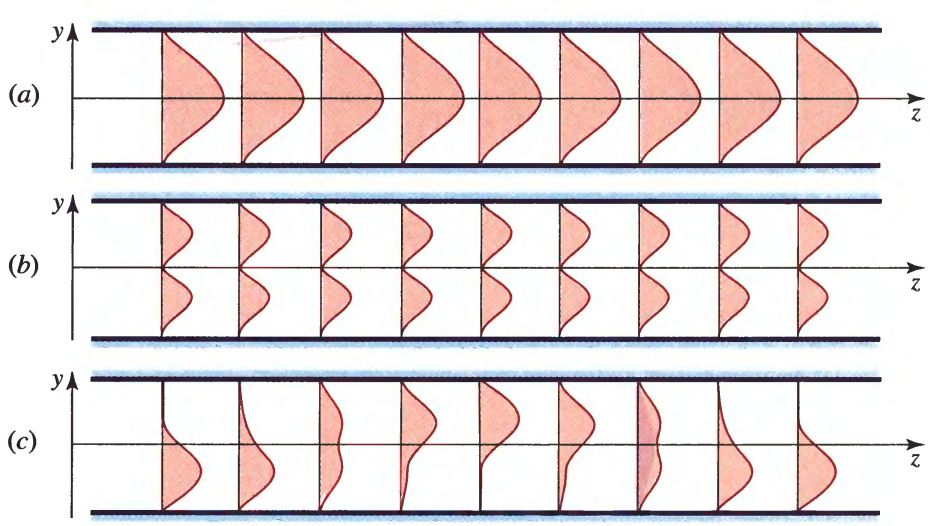

Figure 8.1-8 Variation of the intensity distribution in the transverse direction y at different axial distances z. (*a*) The electric-field complex amplitude in mode 1 is $E(y,z) = u_1(y)\exp(-j\beta_1 z)$, where $u_1(y) = \sqrt{2/d}\cos(\pi y/d)$. The intensity does not vary with z. (*b*) The complex amplitude in mode 2 is $E(y,z) = u_2(y)\exp(-j\beta_2 z)$, where $u_2(y) = \sqrt{2/d}\sin(2\pi y/d)$. The intensity does not vary with z. (*c*) The complex amplitude in a mixture of modes 1 and 2, $E(y,z) = u_1(y)\exp(-j\beta_1 z) + u_2(y)\exp(-j\beta_2 z)$. Since $\beta_1 \neq \beta_2$, the intensity distribution changes with z.

An arbitrary field polarized in the x direction and satisfying the boundary conditions can be written as a weighted superposition of the TE modes,

$$E_x(y,z) = \sum_{m=0}^{M} a_m u_m(y) \exp(-j\beta_m z), \tag{8.1-18}$$

where a_m, the superposition weights, are the amplitudes of the different modes.

EXERCISE 8.1-2

Optical Power in a Multimode Field. Show that the optical power flow in the z direction associated with the multimode field in (8.1-18) is the sum of the powers $(|a_m|^2/2\eta)\cos\theta_m$ carried by each of the modes.

8.2 PLANAR DIELECTRIC WAVEGUIDES

A planar dielectric waveguide is a slab of dielectric material surrounded by media of lower refractive indexes. The light is guided inside the slab by total internal reflection. In thin-film devices the slab is called the "film" and the upper and lower media are called the "cover" and the "substrate," respectively. The inner medium and outer media may also be called the "core" and the "cladding" of the waveguide, respectively. In this section we study the propagation of light in a symmetric planar dielectric waveguide made of a slab of width d and refractive index n_1 surrounded by a cladding of smaller refractive index n_2, as illustrated in Fig. 8.2-1. All materials are assumed to be lossless.

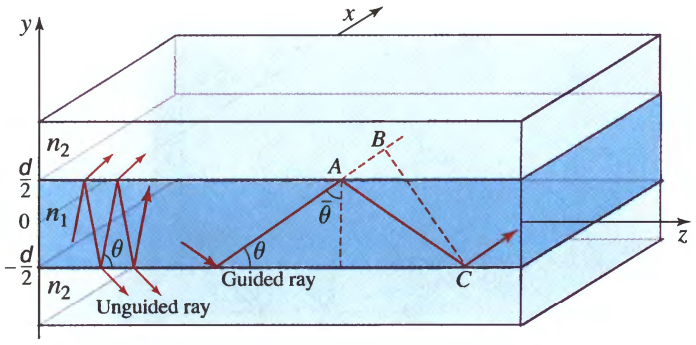

Figure 8.2-1 Planar dielectric (slab) waveguide. Rays making an angle $\theta < \bar{\theta}_c = \cos^{-1}(n_2/n_1)$ are guided by total internal reflection.

Light rays making angles θ with the z axis, in the y–z plane, undergo multiple total internal reflections at the slab boundaries, provided that θ is smaller than the complement of the critical angle $\bar{\theta}_c = \pi/2 - \sin^{-1}(n_2/n_1) = \cos^{-1}(n_2/n_1)$ [see (1.2-5) and Figs. 6.2-3 and 6.2-5]. They travel in the z direction by bouncing between the slab surfaces without loss of power. Rays making larger angles refract, losing a portion of their power at each reflection, and eventually vanish.

To determine the waveguide modes, a formal approach may be pursued by developing solutions to Maxwell's equations in the inner and outer media with the appropriate boundary conditions imposed (see Prob. 8.2-6). We shall instead write the solution in terms of TEM plane waves bouncing between the surfaces of the slab. By imposing the

self-consistency condition, we determine the bounce angles of the waveguide modes from which the propagation constants, field distributions, and group velocities are determined. The analysis is analogous to that used in the previous section for the planar-mirror waveguide.

A. Waveguide Modes

Assume that the field in the slab is in the form of a monochromatic TEM plane wave of wavelength $\lambda = \lambda_o/n_1$ bouncing back and forth at an angle θ smaller than the complementary critical angle $\overline{\theta}_c$. The wave travels with a phase velocity $c_1 = c_o/n_1$, has a wavenumber $n_1 k_o$, and has wavevector components $k_x = 0$, $k_y = n_1 k_o \sin\theta$, and $k_z = n_1 k_o \cos\theta$. To determine the modes we impose the self-consistency condition that a wave reproduces itself after each round trip.

In one round trip, the twice-reflected wave lags behind the original wave by a distance $\overline{AC} - \overline{AB} = 2d \sin\theta$, as in Fig. 8.1-2. There is also a phase φ_r introduced by each internal reflection at the dielectric boundary (see Sec. 6.2). For self-consistency, the phase shift between the two waves must be zero or a multiple of 2π,

$$\frac{2\pi}{\lambda} 2d \sin\theta - 2\varphi_r = 2\pi m, \qquad m = 0, 1, 2, \ldots \tag{8.2-1}$$

or

$$2k_y d - 2\varphi_r = 2\pi m. \tag{8.2-2}$$

The only difference between this condition and the corresponding condition in the mirror waveguide, (8.1-1) and (8.1-3), is that the phase shift π introduced by the mirror is replaced here by the phase shift φ_r introduced at the dielectric boundary.

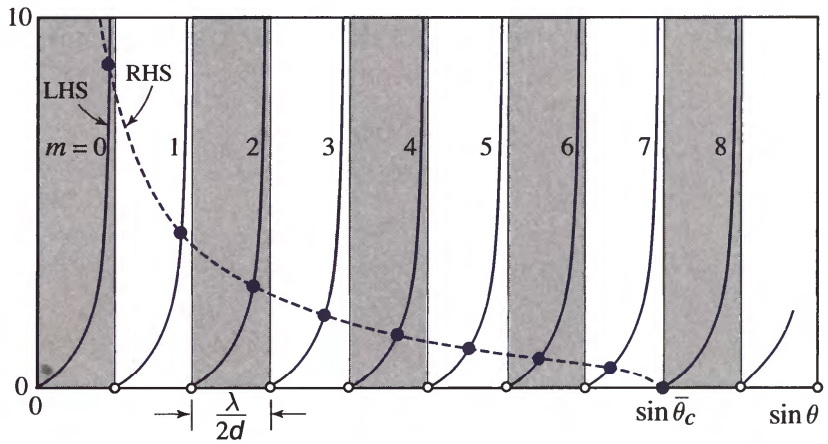

Figure 8.2-2 Graphical solution of (8.2-4) to determine the bounce angles θ_m of the modes of a planar dielectric waveguide. The RHS and LHS of (8.2-4) are plotted versus $\sin\theta$. The intersection points, marked by filled circles, determine $\sin\theta_m$. Each branch of the tan or cot function in the LHS corresponds to a mode. In this plot $\sin\overline{\theta}_c = 8(\lambda/2d)$ and the number of modes is $M = 9$. The open circles mark $\sin\theta_m = m\lambda/2d$, which provide the bounce angles of the modes of a planar-mirror waveguide of the same dimensions.

The reflection phase shift φ_r is a function of the angle θ. It also depends on the polarization of the incident wave, TE or TM. In the TE case (the electric field is in the

x direction), substituting $\theta_1 = \pi/2 - \theta$ and $\theta_c = \pi/2 - \bar{\theta}_c$ in (6.2-11) gives

$$\tan\frac{\varphi_r}{2} = \sqrt{\frac{\sin^2\bar{\theta}_c}{\sin^2\theta} - 1}, \tag{8.2-3}$$

so that φ_r varies from π to 0 as θ varies from 0 to $\bar{\theta}_c$. Rewriting (8.2-1) in the form $\tan(\pi d \sin\theta/\lambda - m\pi/2) = \tan(\varphi_r/2)$ and using (8.2-3), we obtain

$$\boxed{\tan\left(\pi\frac{d}{\lambda}\sin\theta - m\frac{\pi}{2}\right) = \sqrt{\frac{\sin^2\bar{\theta}_c}{\sin^2\theta} - 1}.} \tag{8.2-4}$$

Self-Consistency Condition (TE Modes)

This is a transcendental equation in one variable, $\sin\theta$. Its solutions yield the bounce angles θ_m of the modes. A graphic solution is instructive. The right- and left-hand sides of (8.2-4) are plotted in Fig. 8.2-2 as functions of $\sin\theta$. Solutions are given by the intersection points. The right-hand side (RHS), $\tan(\varphi_r/2)$, is a monotonic decreasing function of $\sin\theta$ that reaches 0 when $\sin\theta = \sin\bar{\theta}_c$. The left-hand side (LHS) generates two families of curves, $\tan[(\pi d/\lambda)\sin\theta]$ and $\cot[(\pi d/\lambda)\sin\theta]$, when m is even and odd, respectively. The intersection points determine the angles θ_m of the modes. The bounce angles of the modes of a *mirror* waveguide of mirror separation d may be obtained from this diagram by using $\varphi_r = \pi$ or, equivalently, $\tan(\varphi_r/2) = \infty$. For comparison, these angles are marked by open circles.

The angles θ_m lie between 0 and $\bar{\theta}_c$. They correspond to wavevectors with components $(0,\ n_1k_o\sin\theta_m,\ n_1k_o\cos\theta_m)$. The z components are the propagation constants

$$\boxed{\beta_m = n_1k_o\cos\theta_m.} \tag{8.2-5}$$

Propagation Constants

Since $\cos\theta_m$ lies between 1 and $\cos\bar{\theta}_c = n_2/n_1$, β_m lies between n_2k_o and n_1k_o, as illustrated in Fig. 8.2-3.

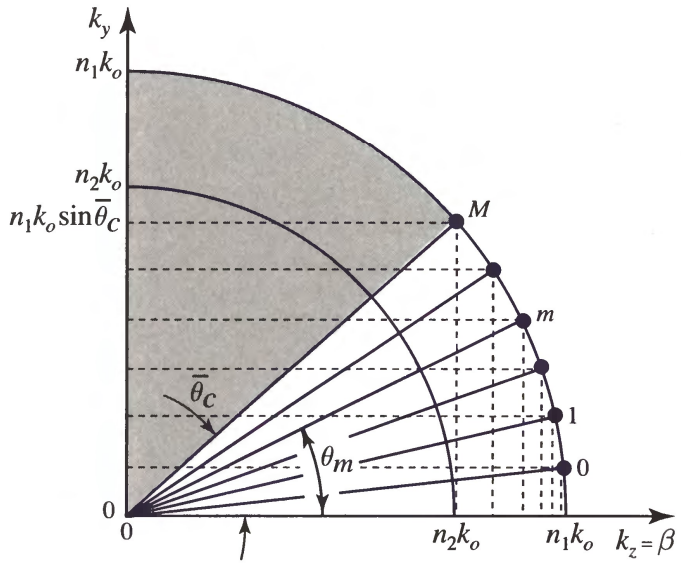

Figure 8.2-3 The bounce angles θ_m and the corresponding components k_z and k_y of the wavevector of the waveguide modes are indicated by dots. The angles θ_m lie between 0 and $\bar{\theta}_c$, and the propagation constants β_m lie between n_2k_o and n_1k_o. These results should be compared with those shown in Fig. 8.1-3 for the planar-mirror waveguide.

The bounce angles θ_m and the propagation constants β_m of TM modes can be found by using the same equation (8.2-1), but with the phase shift φ_r given by (6.2-13). Similar results are obtained.

Number of Modes

To determine the number of TE modes supported by the dielectric waveguide we examine the diagram in Fig. 8.2-2. The abscissa is divided into equal intervals of width $\lambda/2d$, each of which contains a mode marked by a filled circle. This extends over angles for which $\sin\theta \leq \sin\bar{\theta}_c$. The number of TE modes is therefore the smallest integer greater than $\sin\bar{\theta}_c/(\lambda/2d)$, so that

$$M \doteq \frac{\sin\bar{\theta}_c}{\lambda/2d}. \tag{8.2-6}$$

The symbol $\doteq$ denotes that $\sin\bar{\theta}_c/(\lambda/2d)$ is increased to the nearest integer. For example, if $\sin\bar{\theta}_c/(\lambda/2d) = 0.9$, 1, or 1.1, then $M = 1$, 2, and 2, respectively. Substituting $\cos\bar{\theta}_c = n_2/n_1$ into (8.2-6), we obtain

$$\boxed{M \doteq \frac{2d}{\lambda_o}\,\mathrm{NA},} \tag{8.2-7}$$

Number of TE Modes

where

$$\boxed{\mathrm{NA} = \sqrt{n_1^2 - n_2^2}} \tag{8.2-8}$$

Numerical Aperture

is the numerical aperture of the waveguide (the NA is the sine of the angle of acceptance of rays from air into the slab; see Exercise 1.2-5). A similar expression can be obtained for the TM modes. If $d/\lambda_o = 10$, $n_1 = 1.47$, and $n_2 = 1.46$, for example, then $\bar{\theta}_c = 6.7°$, NA $= 0.171$, and $M = 4$ TE modes.

When $\lambda/2d > \sin\bar{\theta}_c$ or $(2d/\lambda_o)\mathrm{NA} < 1$, only one mode is allowed. The waveguide is then a **single-mode waveguide**. This occurs when the slab is sufficiently thin or the wavelength is sufficiently long. Unlike the mirror waveguide, the dielectric waveguide has no absolute cutoff wavelength (or cutoff frequency). In a dielectric waveguide there is at least one TE mode, since the fundamental mode $m = 0$ is always allowed. Each of the modes $m = 1, 2, \ldots$ has its own cutoff wavelength, however.

Stated in terms of frequency, the condition for single-mode operation is that $\nu > \nu_c$, or $\omega > \omega_c$, where the mode cutoff frequency is

$$\boxed{\nu_c = \omega_c/2\pi = \frac{1}{\mathrm{NA}}\,\frac{c_o}{2d}.} \tag{8.2-9}$$

Mode Cutoff Frequency

The number of modes is then $M \doteq \nu/\nu_c = \omega/\omega_c$, which is the relation illustrated in Fig. 8.2-4. M is incremented by unity as ω increases by ω_c. Identical expressions for the number of TM modes are obtained via a similar derivation.

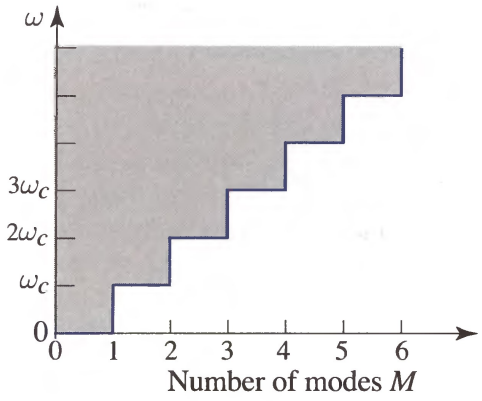

Figure 8.2-4 Number of TE modes as a function of frequency. Compare with Fig. 8.1-5(*a*) for the planar-mirror waveguide. There is no forbidden band in the case at hand.

EXAMPLE 8.2-1. ***Modes in an AlGaAs Waveguide.*** A waveguide is made by sandwiching a layer of $Al_xGa_{1-x}As$ between two layers of $Al_yGa_{1-y}As$. By changing the concentrations of x, y of Al in these compounds their refractive indexes are controlled. If x and y are chosen such that at an operating wavelength $\lambda_o = 0.9$ μm, $n_1 = 3.5$, and $n_1 - n_2 = 0.05$, then for a thickness $d = 10$ μm there are $M = 14$ TE modes. For $d < 0.76$ μm, only a single mode is allowed.

B. Field Distributions

We now determine the field distributions of the TE modes.

Internal Field

The field inside the slab is composed of two TEM plane waves traveling at angles θ_m and $-\theta_m$ with the z axis with wavevector components $(0, \pm n_1 k_o \sin\theta_m, n_1 k_o \cos\theta_m)$. They have the same amplitude and phase shift $m\pi$ (half that of a round trip) at the center of the slab. The electric-field complex amplitude is therefore $E_x(y,z) = a_m u_m(y) \exp(-j\beta_m z)$, where $\beta_m = n_1 k_o \cos\theta_m$ is the propagation constant, a_m is a constant,

$$u_m(y) \propto \begin{cases} \cos\left(2\pi \dfrac{\sin\theta_m}{\lambda} y\right), & m = 0, 2, 4, \ldots \\ \sin\left(2\pi \dfrac{\sin\theta_m}{\lambda} y\right), & m = 1, 3, 5, \ldots, \end{cases} \qquad -\frac{d}{2} \le y \le \frac{d}{2}, \tag{8.2-10}$$

and $\lambda = \lambda_o / n_1$. Note that although the field is harmonic, it does not vanish at the slab boundary. As m increases, $\sin\theta_m$ increases, so that higher-order modes vary more rapidly with y.

External Field

The external field must match the internal field at all boundary points $y = \pm d/2$. It must therefore vary with z as $\exp(-j\beta_m z)$. Substituting $E_x(y,z) = a_m u_m(y) \exp(-j\beta_m z)$ into the Helmholtz equation $(\nabla^2 + n_2^2 k_o^2) E_x(y,z) = 0$, we obtain

$$\frac{d^2 u_m}{dy^2} - \gamma_m^2 u_m = 0, \tag{8.2-11}$$

where

$$\gamma_m^2 = \beta_m^2 - n_2^2 k_o^2. \tag{8.2-12}$$

Since $\beta_m > n_2 k_o$ for guided modes (See Fig. 8.2-3), $\gamma_m^2 > 0$, so that (8.2-11) is satisfied by the exponential functions $\exp(-\gamma_m y)$ and $\exp(\gamma_m y)$. Since the field must decay away from the slab, we choose $\exp(-\gamma_m y)$ in the upper medium and $\exp(\gamma_m y)$ in the lower medium

$$u_m(y) \propto \begin{cases} \exp(-\gamma_m y), & y > d/2 \\ \exp(\gamma_m y), & y < -d/2. \end{cases} \tag{8.2-13}$$

The decay rate γ_m is known as the **extinction coefficient**. The wave is said to be an **evanescent wave**. Substituting $\beta_m = n_1 k_o \cos\theta_m$ and $\cos\bar{\theta}_c = n_2/n_1$ into (8.2-12), we obtain

$$\boxed{\gamma_m = n_2 k_o \sqrt{\frac{\cos^2\theta_m}{\cos^2\bar{\theta}_c} - 1}\,.} \tag{8.2-14}$$

Extinction Coefficient

As the mode number m increases, θ_m increases, and γ_m decreases. Higher-order modes therefore penetrate deeper into the cover and substrate.

To determine the proportionality constants in (8.2-10) and (8.2-13), we match the internal and external fields at $y = d/2$ and use the normalization

$$\int_{-\infty}^{\infty} u_m^2(y)\, dy = 1. \tag{8.2-15}$$

This gives an expression for $u_m(y)$ valid for all y. These functions are illustrated in Fig. 8.2-5. As in the mirror waveguide, all of the $u_m(y)$ are orthogonal, i.e.,

$$\int_{-\infty}^{\infty} u_m(y)\, u_l(y)\, dy = 0, \qquad l \neq m. \tag{8.2-16}$$

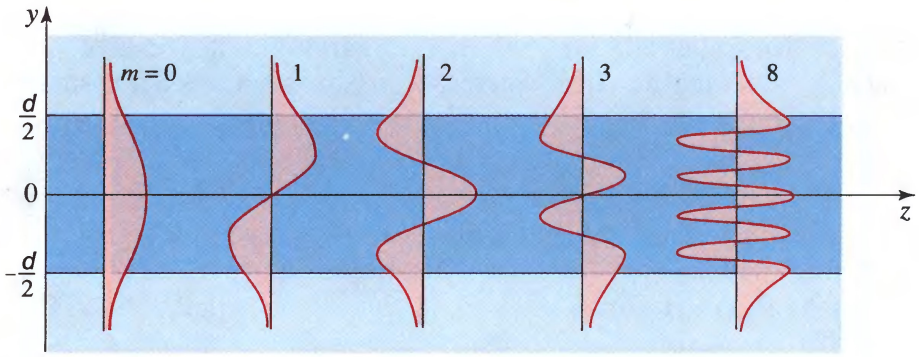

Figure 8.2-5 Field distributions for TE guided modes in a dielectric waveguide. These results should be compared with those shown in Fig. 8.1-4 for the planar-mirror waveguide.

An arbitrary TE field in the dielectric waveguide can be written as a superposition of these modes:

$$E_x(y,z) = \sum_m a_m u_m(y) \exp(-j\beta_m z), \tag{8.2-17}$$

where a_m is the amplitude of mode m.

EXERCISE 8.2-1

Confinement Factor. The power confinement factor is the ratio of power in the slab to the total power

$$\Gamma_m = \frac{\int_0^{d/2} u_m^2(y)\,dy}{\int_0^{\infty} u_m^2(y)\,dy}. \tag{8.2-18}$$

Derive an expression for Γ_m as a function of the angle θ_m and the ratio d/λ. Demonstrate that the lowest-order mode (smallest θ_m) has the highest power confinement factor.

The field distributions of the TM modes may be similarly determined (Fig. 8.2-6). Since it is parallel to the slab boundary, the z component of the electric field behaves similarly to the x component of the TE electric field. The analysis may start by determining $E_z(y,z)$. Using the properties of the constituent TEM waves, the other components $E_y(y,z)$ and $H_x(y,z)$ may readily be determined, as was done for mirror waveguides. Alternatively, Maxwell's equations may be used to determine these fields.

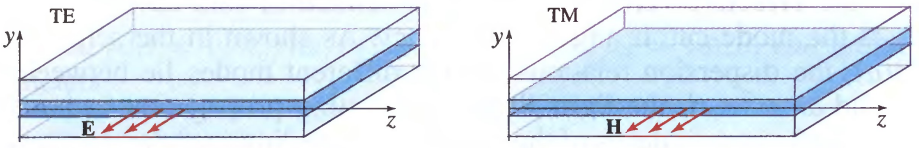

Figure 8.2-6 TE and TM modes in a dielectric planar waveguide.

The field distribution of the lowest-order TE mode ($m = 0$) is similar in shape to that of the Gaussian beam (see Chapter 3). However, unlike the Gaussian beam, guided light does not spread in the transverse direction as it propagates in the axial direction (see Fig. 8.2-7). In a waveguide, the tendency of light to diffract is compensated by the guiding action of the medium.

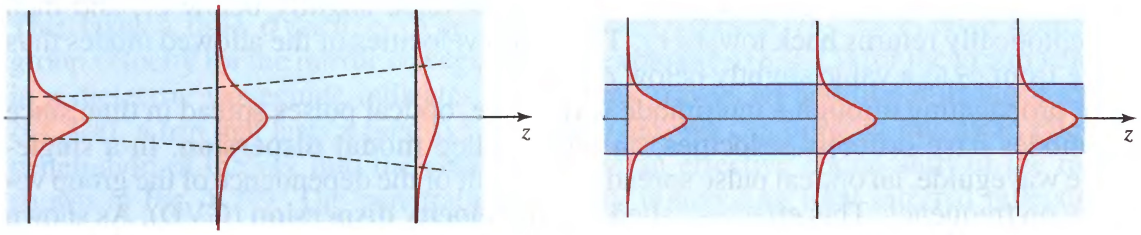

(*a*) (*b*)

Figure 8.2-7 (*a*) Gaussian beam in a homogeneous medium. (*b*) Guided mode in a dielectric waveguide.

C. Dispersion Relation and Group Velocities

The dispersion relation (ω versus β) is obtained by writing the self-consistency equation (8.2-2) in terms of β and ω. Since $k_y^2 = (\omega/c_1)^2 - \beta^2$, (8.2-2) gives

$$2d\sqrt{\frac{\omega^2}{c_1^2} - \beta^2} = 2\varphi_r + 2\pi m. \tag{8.2-19}$$

Since $\cos\theta = \beta/(\omega/c_1)$ and $\cos\bar{\theta}_c = n_2/n_1 = c_1/c_2$, (8.2-3) becomes

$$\tan^2\frac{\varphi_r}{2} = \frac{\beta^2 - \omega^2/c_2^2}{\omega^2/c_1^2 - \beta^2}. \tag{8.2-20}$$

Substituting (8.2-20) into (8.2-19) we obtain

$$\boxed{\tan^2\left(\frac{d}{2}\sqrt{\frac{\omega^2}{c_1^2} - \beta^2} - m\frac{\pi}{2}\right) = \frac{\beta^2 - \omega^2/c_2^2}{\omega^2/c_1^2 - \beta^2}.} \tag{8.2-21}$$

Dispersion Relation

This relation may be plotted by rewriting it in parametric form,

$$\frac{\omega}{\omega_c} = \frac{\sqrt{n_1^2 - n_2^2}}{\sqrt{n_1^2 - n^2}}\left(m + \frac{2}{\pi}\tan^{-1}\sqrt{\frac{n^2 - n_2^2}{n_1^2 - n^2}}\right), \quad \beta = n\omega/c_o, \tag{8.2-22}$$

in terms of the **effective refractive index** n defined in (8.2-22), where $\omega_c/2\pi = c_o/2d\,\mathrm{NA}$ is the mode-cutoff angular frequency. As shown in the schematic plot in Fig. 8.2-8(a), the dispersion relations for the different modes lie between the lines $\omega = c_2\beta$ and $\omega = c_1\beta$, the **light lines** representing propagation in homogeneous media with the refractive indexes of the surrounding medium and the slab, respectively. As the frequency increases above the mode cutoff frequency, the dispersion relation moves from the light line of the surrounding medium toward the light line of the slab, i.e., the effective refractive index n increases from n_2 to n_1. This effect is indicative of a stronger confinement of waves of shorter wavelength in the medium of higher refractive index.

The group velocity is obtained from the dispersion relation by determining the slope $v = d\omega/d\beta$ for each of the guided modes. The dependence of the group velocity on the angular frequency is illustrated schematically in Fig. 8.2-8(b). As the angular frequency increases above the mode cutoff frequency for each mode, the group velocity decreases from its maximum value c_2, reaches a minimum value slightly below c_1, and then asymptotically returns back toward c_1. The group velocities of the allowed modes thus range from c_2 to a value slightly below c_1.

In propagating through a multimode waveguide, optical pulses spread in time since the modes have different velocities, an effect called **modal dispersion**. In a single-mode waveguide, an optical pulse spreads as a result of the dependence of the group velocity on frequency. This effect is called **group velocity dispersion** (GVD). As shown in Sec. 5.6, GVD occurs in homogeneous materials by virtue of the frequency dependence of the refractive index of the material. Moreover, GVD occurs in waveguides even in the absence of material dispersion. It is then a consequence of the frequency dependence of the propagation coefficients, which are determined by the dependence of wave confinement on wavelength. As illustrated in Fig. 8.2-8(b), each mode has

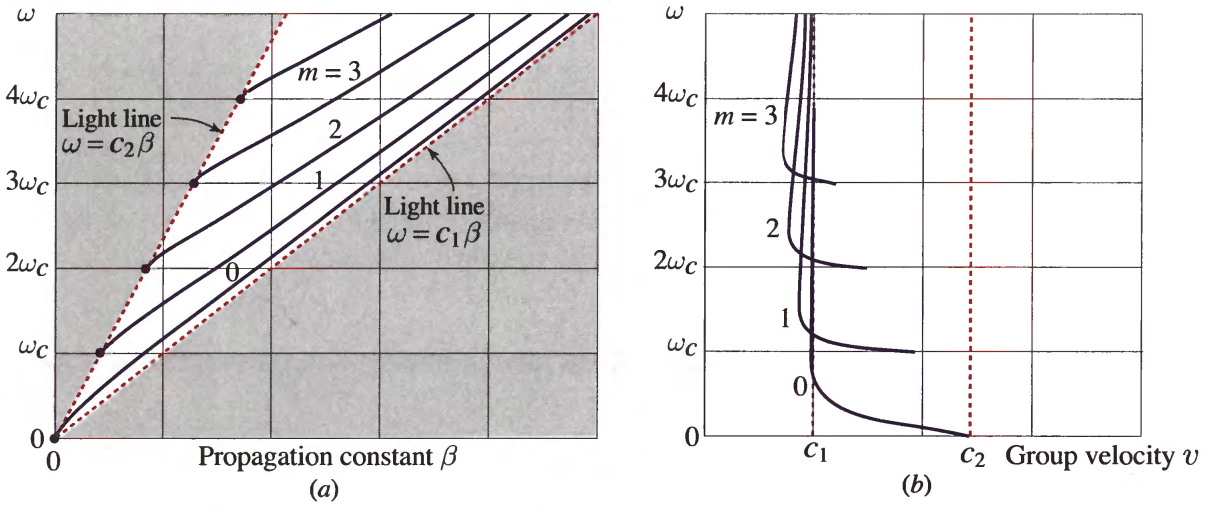

Figure 8.2-8 Schematic representations of (a) the dispersion relation for the different TE modes, $m = 0, 1, 2, \ldots$; and (b) the frequency dependence of the group velocity, which is the derivative of the dispersion relation, $v = d\omega/d\beta$.

a particular angular frequency at which the group velocity changes slowly with frequency (the point at which v reaches its minimum value so that its derivative with respect to ω is zero). At this frequency, the GVD coefficient is zero and pulse spreading is negligible.

An approximate expression for the group velocity may be obtained by taking the total derivative of (8.2-19) with respect to β,

$$\frac{2d}{2k_y}\left(\frac{2\omega}{c_1^2}\frac{d\omega}{d\beta} - 2\beta\right) = 2\frac{\partial\varphi_r}{\partial\beta} + 2\frac{\partial\varphi_r}{\partial\omega}\frac{d\omega}{d\beta}. \tag{8.2-23}$$

Substituting $d\omega/d\beta = v$, $k_y/(\omega/c_1) = \sin\theta$, and $k_y/\beta = \tan\theta$, and introducing the new parameters

$$\Delta z = \frac{\partial\varphi_r}{\partial\beta}, \qquad \Delta\tau = -\frac{\partial\varphi_r}{\partial\omega}, \tag{8.2-24}$$

we obtain

$$v = \frac{d\cot\theta + \Delta z}{d\csc\theta/c_1 + \Delta\tau}. \tag{8.2-25}$$

As we recall from (8.1-14) and Fig. 8.1-6 for the planar-mirror waveguide, $d\cot\theta$ is the distance traveled in the z direction as a ray travels once between the two boundaries. This takes a time $d\csc\theta/c_1$. The ratio $d\cot\theta/(d\csc\theta)/c_1 = c_1\cos\theta$ yields the group velocity for the mirror waveguide. The expression (8.2-25) for the group velocity in a dielectric waveguide indicates that the ray travels an additional distance $\Delta z = \partial\varphi_r/\partial\beta$, a trip that lasts a time $\Delta\tau = -\partial\varphi_r/\partial\omega$. We can think of this as an effective penetration of the ray into the cladding, or as an effective lateral shift of the ray, as shown in Fig. 8.2-9. The penetration of a ray undergoing total internal reflection is known as the **Goos–Hänchen effect** (see Prob. 6.2-7). Using (8.2-24) it can be shown that $\Delta z/\Delta\tau = \omega/\beta = c_1/\cos\theta$.

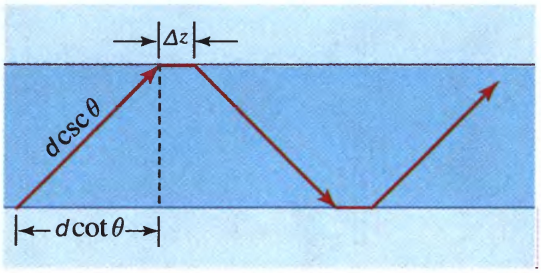

Figure 8.2-9 A ray model that replaces the reflection phase shift with an additional distance Δz traversed at velocity $c_1/\cos\theta$.

EXERCISE 8.2-2

The Asymmetric Planar Waveguide. Examine the TE field in an asymmetric planar waveguide consisting of a dielectric slab of width d and refractive index n_1 placed on a substrate of lower refractive index n_2 and covered with a medium of refractive index $n_3 < n_2 < n_1$, as illustrated in Fig. 8.2-10.

(a) Determine an expression for the maximum inclination angle θ of plane waves undergoing total internal reflection, and the corresponding numerical aperture NA of the waveguide.

(b) Write an expression for the self-consistency condition, similar to (8.2-4).

(c) Determine an approximate expression for the number of modes M (valid when M is very large).

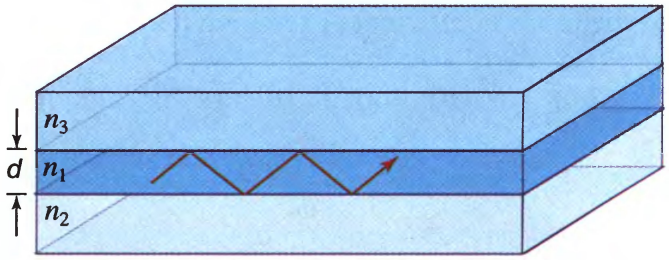

Figure 8.2-10 Asymmetric planar waveguide.

8.3 TWO-DIMENSIONAL WAVEGUIDES

The planar-mirror waveguide and the planar dielectric waveguide studied in the preceding two sections confine light in one transverse direction (the y direction) while guiding it along the z direction. Two-dimensional waveguides confine light in the two transverse directions (the x and y directions). The principle of operation and the underlying modal structure of two-dimensional waveguides is basically the same as planar waveguides; only the mathematical description is lengthier. This section is a brief description of the nature of modes in two-dimensional waveguides. Details can be found in specialized books. Chapter 9 is devoted to an important example of two-dimensional waveguides, the cylindrical dielectric waveguide used in optical fibers.

Rectangular Mirror Waveguide

The simplest generalization of the planar waveguide is the rectangular waveguide (Fig. 8.3-1). If the walls of the waveguide are mirrors, then, as in the planar case, light is guided by multiple reflections at all angles. For simplicity, we assume that the cross section of the waveguide is a square of width d. If a plane wave of wavevector (k_x, k_y, k_z) and its multiple reflections are to exist self-consistently inside the waveg-

uide, it must satisfy the conditions:

$$\begin{aligned} 2k_x d &= 2\pi m_x, \qquad m_x = 1, 2, \ldots \\ 2k_y d &= 2\pi m_y, \qquad m_y = 1, 2, \ldots, \end{aligned} \tag{8.3-1}$$

which are obvious generalizations of (8.1-3).

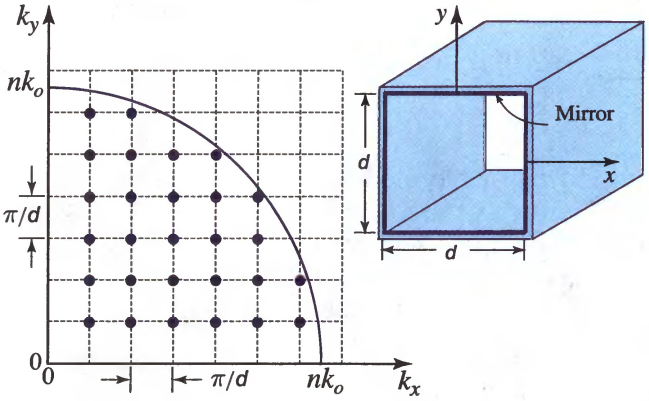

Figure 8.3-1 Modes of a rectangular mirror waveguide are characterized by a finite number of discrete values of k_x and k_y represented by dots.

The propagation constant $\beta = k_z$ can be determined by k_x and k_y by using the relation $k_x^2 + k_y^2 + \beta^2 = n^2 k_o^2$. The three components of the wavevector therefore have discrete values, yielding a finite number of modes. Each mode is identified by two indexes m_x and m_y (instead of one index m). All positive integer values of m_x and m_y are allowed as long as $k_x^2 + k_y^2 \leq n^2 k_o^2$, as illustrated in Fig. 8.3-1.

The number of modes M can be easily determined by counting the number of dots within a quarter circle of radius nk_o in the k_x versusk_y diagram (Fig. 8.3-1). If this number is large, it may be approximated by the ratio of the area $\pi(nk_o)^2/4$ to the area of a unit cell $(\pi/d)^2$,

$$M \approx \frac{\pi}{4}\left(\frac{2d}{\lambda}\right)^2. \tag{8.3-2}$$

Since there are two polarizations per mode, the total number of modes is actually $2M$. Comparing this to the number of modes in a one-dimensional mirror waveguide, $M \approx 2d/\lambda$, we see that increase of the dimensionality yields approximately the square of the number of modes. The number of modes is a measure of the degrees of freedom. When we add a second dimension we simply multiply the number of degrees of freedom.

The field distributions associated with these modes are generalizations of those in the planar case. Patterns such as those in Fig. 8.1-4 are obtained in each of the x and y directions depending on the mode indexes m_x and m_y.

Rectangular Dielectric Waveguide

A dielectric cylinder of refractive index n_1 with square cross section of width d is embedded in a medium of slightly lower refractive index n_2. The waveguide nodes can be determined using a similar theory. Components of the wavevector (k_x, k_y, k_z) must satisfy the condition $k_x^2 + k_y^2 \leq n_1^2 k_o^2 \sin^2 \overline{\theta}_c$, where $\overline{\theta}_c = \cos^{-1}(n_2/n_1)$, so that k_x and k_y lie in the area shown in Fig. 8.3-2. The values of k_x and k_y for the different modes can be obtained from a self-consistency condition in which the phase shifts at the dielectric boundary are included, as was done in the planar case.

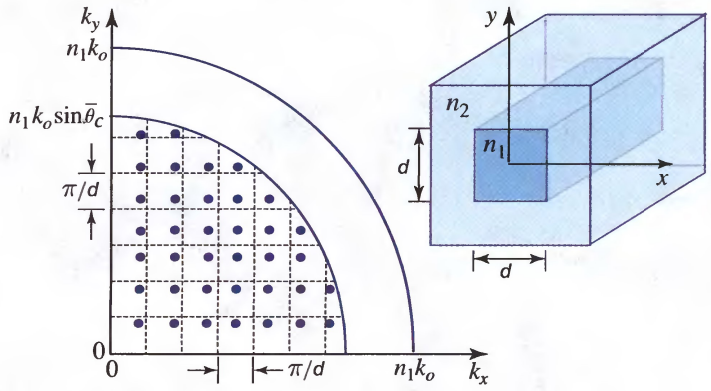

Figure 8.3-2 Geometry of a rectangular dielectric waveguide. The values of k_x and k_y for the waveguide modes are marked by dots.

Unlike the mirror waveguide, k_x and k_y of the modes are not uniformly spaced. However, two consecutive values of k_x (or k_y) are separated by an *average* value of π/d (the same as for the mirror waveguide). The number of modes can therefore be approximated by counting the number of dots in the inner circle in the k_x versusk_y diagram of Fig. 8.3-2, assuming an average spacing of π/d. The result is $M \approx (\pi/4)(n_1 k_o \sin\bar{\theta}_c)^2/(\pi/d)^2$, from which

$$M \approx \frac{\pi}{4}\left(\frac{2d}{\lambda_o}\right)^2 (\text{NA})^2, \qquad (8.3\text{-}3)$$

Number of TE Modes

where NA $= \sqrt{n_1^2 - n_2^2}$ is the numerical aperture. The approximation is satisfactory when M is large. There is also an identical number M of TM modes. The number of modes is roughly the square of that for the planar dielectric waveguide (8.2-7).

Geometries of Channel Waveguides

Useful geometries for waveguides include the strip, the embedded-strip, the rib or ridge, and the strip-loaded waveguides illustrated in Fig. 8.3-3. The exact analysis for some of these geometries is not easy, and approximations are usually used. The reader is referred to specialized books for further information about this topic.

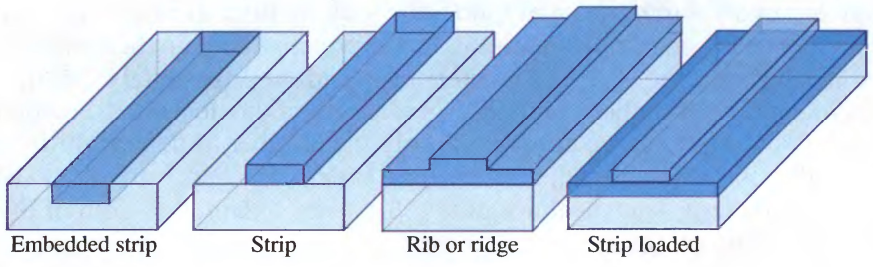

Figure 8.3-3 Various waveguide geometries. The darker the shading, the higher the refractive index.

The waveguide may be fabricated in different configurations, as illustrated in Fig. 8.3-4 for the embedded-strip geometry. S bends are used to offset the propagation axis. The Y branch plays the role of a beamsplitter or combiner. Two Y branches may be used to make a Mach–Zehnder interferometer. Two waveguides in close proximity, or intersecting, can exchange power and may be used as directional couplers, as we shall see in the next section.

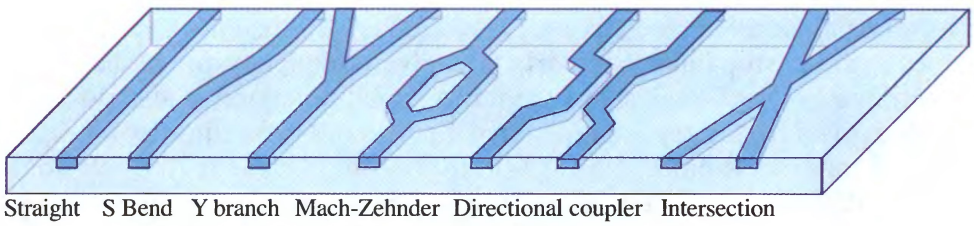

Figure 8.3-4 Different configurations for waveguides.

Materials

The most advanced technology for fabricating waveguides is Ti:$LiNbO_3$. An embedded-strip waveguide is fabricated by diffusing titanium into a lithium niobate substrate to increase its refractive index in the region of the strip. GaAs strip waveguides are made by using layers of GaAs and AlGaAs of lower refractive index. Another semiconductor material that has recently gained importance in waveguides is InP. Glass waveguides are made by ion exchange. Polymer waveguides are also emerging as a viable technology.

Waveguides can also be fabricated using **silicon-on-insulator** (Si-SiO_2 or SOI), and silicon and oxide etching tools, which are standards in the industry. This technology is also called **silica-on-silicon**. Since the refractive index of silica is $\sim$ 3.5 and that of silica is less than 1.5, this combination of materials exhibits a large index-of-refraction difference Δn. A typical SOI may take the form of a silicon rib waveguide (see Fig. 8.3-3) on top of a layer of silica, serving as a cladding, with a silicon substrate underneath. Silicon processing and fabrication has been well developed by the microelectronics industry, and compatibility with CMOS fabrication technology is an important advantage.

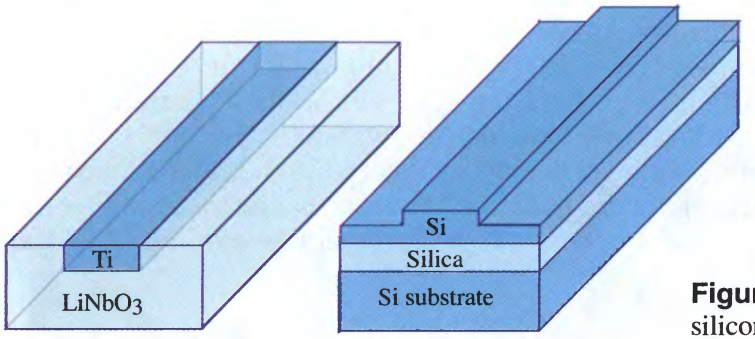

Figure 8.3-5 $LiNbO_3$ and silica-on-silicon waveguides.

The ability to modulate the refractive index is an important requirement for materials used in integrated-optic devices, such as light modulators and switches, as we shall see in Chapters 20 and 23.

8.4 PHOTONIC-CRYSTAL WAVEGUIDES

Bragg-Grating Waveguide

We have seen so far that light may be guided by bouncing between two parallel reflectors — e.g., planar mirrors as described in Sec. 8.1; or planar dielectric boundaries, at which the light undergoes total internal reflection, as described in Sec. 8.2. Alternatively, Bragg grating reflectors (BGR) may be used (see Sec. 7.1C), as illustrated in Fig. 8.4-1. The BGR is a stack of alternating dielectric layers that has special angle- and

frequency-dependent reflectance. For a given angle, the reflectance is close to unity at frequencies within a stop band. Similarly, at a given frequency, the reflectance is close to unity within a range of angles, but omnidirectional reflection is also possible. Thus, a wave with a given frequency can be guided through the waveguide by repeated reflections within a range of bounce angles. Within this angular range, the self-consistency condition is satisfied at a discrete set of angles, each corresponding to a propagating mode. The field distribution of a propagating mode is confined principally to the slab; decaying (evanescent) tails reach into the adjacent grating layers, as illustrated in Fig. 8.4-1.

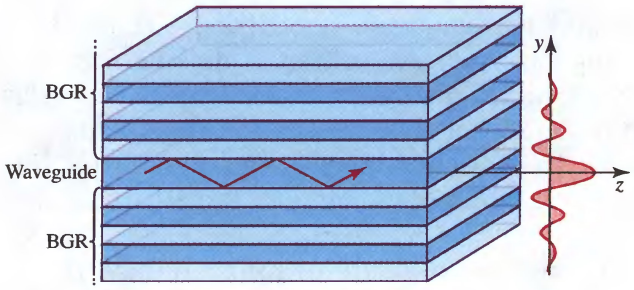

Figure 8.4-1 Planar waveguide made of a dielectric slab sandwiched between two Bragg-grating reflectors (BGR).

Bragg-Grating Waveguide as a Photonic Crystal with a Defect Layer

If the upper and lower gratings of a Bragg-grating waveguide are identical, and the slab thickness is comparable to the thickness of the periodic layers constituting the gratings, then the entire medium may be regarded as a 1D periodic structure, i.e., a 1D photonic crystal, but with a **defect**. For example, the device shown in Fig. 8.4-1 is periodic everywhere except for the slab, which is a layer of different thickness and/or different refractive index; the slab may therefore be viewed as a "defective" layer. As described in Sec. 7.2, a perfect photonic crystal has a dispersion relation, or energy band diagram, containing bandgaps within which no propagating modes exist. In the presence of the "defective" layer, however, a mode whose frequency lies within the bandgap may exist, but it is confined primarily within the layer. Such a mode corresponds to a frequency in the dispersion diagram that lies within the photonic bandgap, as illustrated in Fig. 8.4-2. Such a frequency is the analog of a defect energy level that lies within the bandgap of a semiconductor crystal.

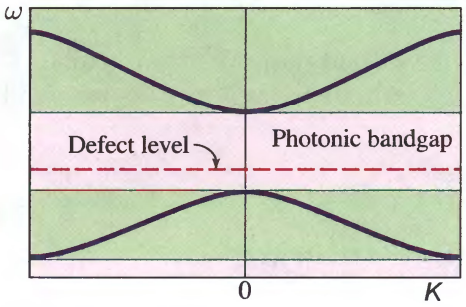

Figure 8.4-2 Dispersion diagram of a photonic crystal with a defect layer.

2D Photonic-Crystal Waveguides

Waveguides may also be created by introducing a path of defects in a 2D photonic crystal. In the example illustrated in Fig. 8.4-3(a), a 2D photonic crystal comprising a set of parallel cylindrical holes, placed in a dielectric material at the points of a periodic

triangular lattice, exhibits a complete photonic bandgap for waves traveling along directions parallel to the plane of periodicity (normal to the cylindrical holes). The defect waveguide takes the form of a line of absent holes. A wave entering the waveguide at frequencies within the photonic bandgap does not leak into the surrounding periodic media so that the light is guided through the waveguide. A typical profile of the field distribution is illustrated in Fig. 8.4-3(a).

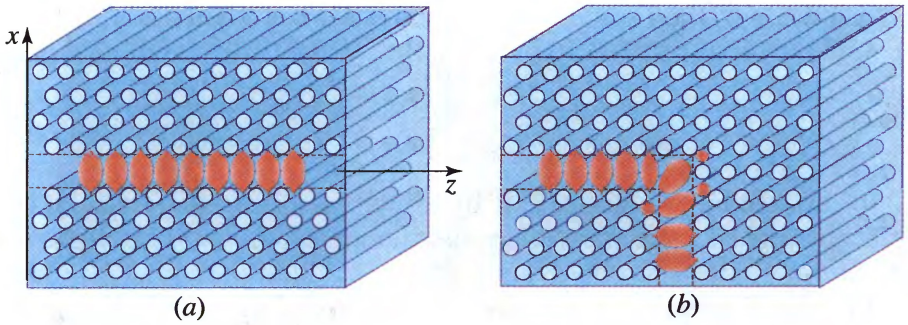

Figure 8.4-3 (a) Propagating mode in a photonic-crystal waveguide. (b) L-shaped photonic-crystal waveguide.

Moreover, because of the omnidirectional nature of the photonic bandgap, light may be guided through photonic-crystal waveguides with sharp bends and corners without losing energy into the surrounding medium, as illustrated by the L-shaped waveguide configuration shown in Fig. 8.4-3(b). Such behavior is not possible with conventional dielectric waveguides based on total internal reflection.

8.5 OPTICAL COUPLING IN WAVEGUIDES

A. Input Couplers

Mode Excitation

As indicated in previous sections, light propagates in a waveguide in the form of modes. The complex amplitude of the optical field is generally a superposition of these modes,

$$E(y,z) = \sum_m a_m u_m(y) \exp(-j\beta_m z), \tag{8.5-1}$$

where a_m is the amplitude, $u_m(y)$ is the transverse distribution (assumed to be real), and β_m is the propagation constant of mode m.

The amplitudes of the different modes depend on the nature of the light source used to excite the waveguide. If the source has a distribution that is a perfect match to a specific mode, only that mode will be excited. In general, a source of arbitrary distribution $s(y)$ excites different modes at different levels. The fraction of power transferred from the source to mode m depends on the degree of similarity between $s(y)$ and $u_m(y)$. To establish this, we write $s(y)$ as an expansion (a weighted superposition) of the orthogonal functions $u_m(y)$,

$$s(y) = \sum_m a_m u_m(y), \tag{8.5-2}$$

where the coefficient a_l, which represents the amplitude of the excited mode l, is

$$a_l = \int_{-\infty}^{\infty} s(y)\, u_l(y)\, dy. \tag{8.5-3}$$

This expression can be derived by multiplying both sides of (8.5-2) by $u_l(y)$, integrating with respect to y, and using the orthogonality relation $\int_{-\infty}^{\infty} u_l(y)\, u_m(y)\, dy = 0$ for $l \neq m$ along with the normalization condition. The coefficient a_l represents the degree of similarity (or correlation) between the source distribution $s(y)$ and the mode distribution $u_l(y)$.

Input Couplers

Light may be coupled into a waveguide by directly focusing it at one end (Fig. 8.5-1). To excite a given mode, the transverse distribution of the incident light $s(y)$ should match that of the mode. The polarization of the incident light must also match that of the desired mode. Because of the small dimensions of the waveguide slab, focusing and alignment are usually difficult and coupling using this method is inefficient.

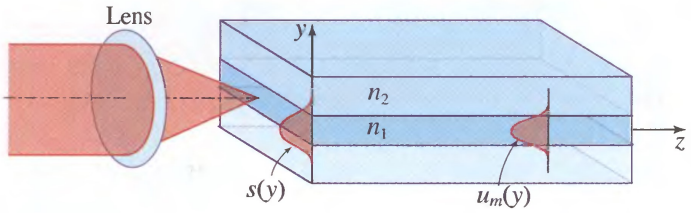

Figure 8.5-1 Coupling an optical beam into an optical waveguide.

In a multimode waveguide, the amount of coupling can be assessed by using a ray-optics approach (Fig. 8.5-2). The guided rays within the waveguide are confined to an angle $\bar{\theta}_c = \cos^{-1}(n_2/n_1)$. Because of refraction at the input to the waveguide, this corresponds to an external angle θ_a satisfying $\text{NA} = \sin\theta_a = n_1 \sin\bar{\theta}_c = n_1\sqrt{1-(n_2/n_1)^2} = \sqrt{n_1^2 - n_2^2}$, where NA is the numerical aperture of the waveguide (see Exercise 1.2-5). For maximum coupling efficiency the incident light should be focused within the angle θ_a.

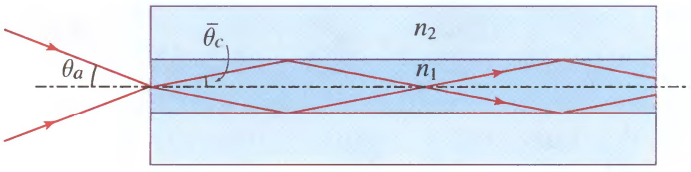

Figure 8.5-2 Focusing rays into a multimode waveguide.

Light may also be coupled from a semiconductor source (a light-emitting diode or a laser diode) into a waveguide by simply aligning the ends of the source and the waveguide, leaving a small space that is selected for maximum coupling (Fig. 8.5-3). In light-emitting diodes, light originates from a semiconductor junction region and is emitted in all directions. In a laser diode, the emitted light is confined in a waveguide of its own (light-emitting diodes and laser diodes are described in Chapter 17). Other methods of coupling light into waveguides include the use of prisms, diffraction gratings, and other waveguides, as discussed below.

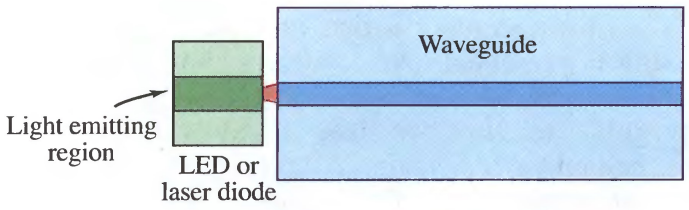

Figure 8.5-3 End butt coupling from a light-emitting diode or laser diode into a waveguide.

Prism and Grating Side Couplers

Can optical power be coupled into a guided mode of a waveguide by use of a source wave entering from the side at some angle θ_i in the cladding, as shown in Fig. 8.5-4(a)? The condition for such coupling is that the axial component of the wavevector of the incident wave, $n_2 k_o \cos\theta_i$, equals the propagation constant β_m of the guided mode. Since $\beta_m > n_2 k_o$ (see Fig. 8.5-4), it is not possible to achieve the required phase matching condition $\beta_m = n_2 k_o \cos\theta_i$. The axial component of the wavevector of the incident wave is simply too small. However, the problem may be alleviated by use of a prism or a grating.

As illustrated in Fig. 8.5-4(b), a prism of refractive index $n_p > n_2$ is placed at a short distance d_p from the waveguide slab. The incident wave is refracted into the prism where it undergoes total internal reflection at an angle θ_p. The incident and reflected waves form a wave traveling in the z direction with propagation constant $\beta_p = n_p k_o \cos\theta_p$. The transverse field distribution extends into the space separating the prism and the slab, as an evanescent wave that decays exponentially. If the distance d_p is sufficiently small, the wave is coupled into a mode of the slab waveguide with a matching propagation constant $\beta_m \approx \beta_p = n_p k_o \cos\theta_p$. Since $n_p > n_2$, phase matching is possible, and if an appropriate interaction distance is selected, significant power can be coupled into the waveguide. The operation may also be reversed to make an output coupler, extracting light from the slab waveguide into free space.

The grating [Fig. 8.5-4(c)] addresses the phase-matching problem by modifying the wavevector of the incoming wave. A grating with period Λ modulates the incoming wave by phase factors $2\pi q/\Lambda z$, where $q = \pm 1, \pm 2, \ldots$. These are equivalent to changes of the axial component of the wavevector by factors $2\pi q/\Lambda$. The phase matching condition can now be satisfied if $n_2 k_o \cos\theta_i + 2\pi q/\Lambda = \beta_m$, with $q = 1$, for example. The grating may even be designed to enhance the $q = 1$ component.

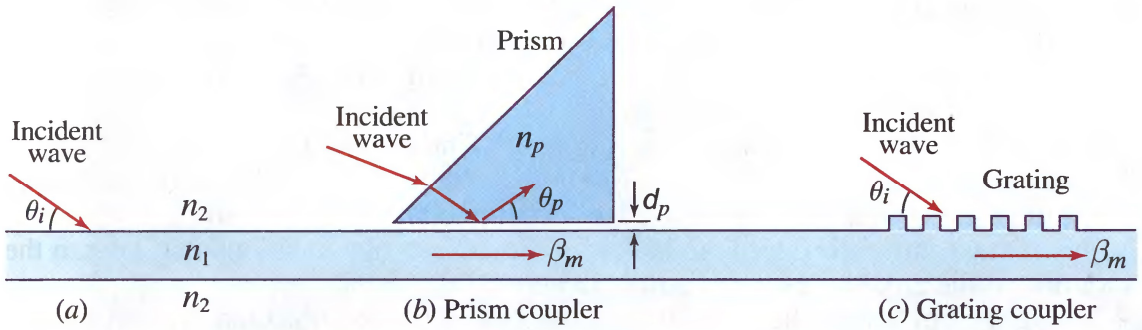

Figure 8.5-4 Prism and grating side couplers.

B. Coupled Waveguides

If two waveguides are sufficiently close such that their fields overlap, light can be coupled from one into the other. Optical power can then be transferred between the

waveguides, an effect that can be used to make optical couplers and switches. The basic principle of waveguide coupling is presented here; couplers and switches are discussed in Chapters 23 and 24.

Consider two parallel planar waveguides made of two slabs of widths d, separation $2a$, and refractive indexes n_1 and n_2, embedded in a medium of refraction index n that is slightly smaller than n_1 and n_2, as illustrated in Fig. 8.5-5. Each of the waveguides is assumed to be single-mode. The separation between the waveguides is such that the optical field outside the slab of one waveguide (in the absence of the other) overlaps slightly with the slab of the other waveguide.

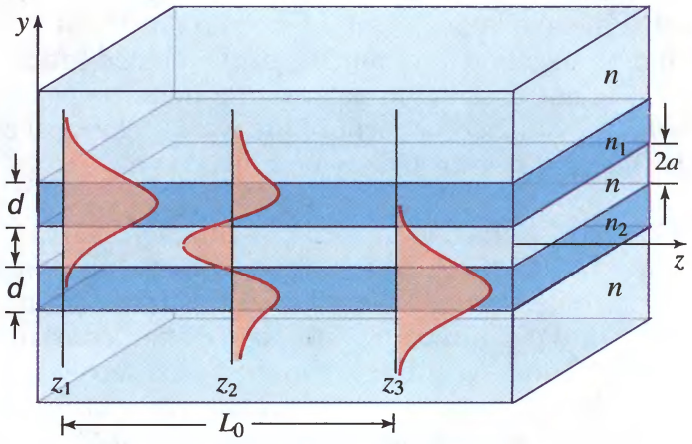

Figure 8.5-5 Coupling between two parallel planar waveguides. At z_1 light is mostly in waveguide 1, at z_2 it is divided equally between the two waveguides, and at z_3 it is mostly in waveguide 2.

The formal approach to studying the propagation of light in this structure is to write Maxwell's equations for the different regions and use the boundary conditions to determine the modes of the overall system. These modes are different from those of each of the waveguides in isolation. An exact analysis is not easy and is beyond the scope of this book. For weak coupling, however, a simplified approximate theory, known as coupled-mode theory, is often satisfactory.

Coupled-mode theory assumes that the mode of each waveguide is determined as if the other waveguide were absent. In the presence of both waveguides, the modes are taken to remain approximately unchanged, say $u_1(y)\exp(-j\beta_1 z)$ and $u_2(y)\exp(-j\beta_2 z)$. Coupling is assumed to modify only the *amplitudes* of these modes without affecting either their transverse spatial distributions or their propagation constants. The amplitudes of the modes of waveguides 1 and 2 are therefore functions of z, $a_1(z)$, and $a_2(z)$. The theory is directed toward determining $a_1(z)$ and $a_2(z)$ under appropriate boundary conditions.

Coupling can be regarded as a scattering effect. The field of waveguide 1 is scattered from waveguide 2, creating a source of light that changes the amplitude of the field in waveguide 2. The field of waveguide 2 has a similar effect on waveguide 1. An analysis of this mutual interaction leads to two coupled differential equations that govern the variation of the amplitudes $a_1(z)$ and $a_2(z)$.

It can be shown (see the derivation at the end of this section) that the amplitudes $a_1(z)$ and $a_2(z)$ are governed by two coupled first-order differential equations

$$\frac{da_1}{dz} = -j\mathcal{C}_{21}\exp(j\,\Delta\beta\, z)\, a_2(z) \tag{8.5-4a}$$

$$\frac{da_2}{dz} = -j\mathcal{C}_{12}\exp(-j\,\Delta\beta\, z)\, a_1(z), \tag{8.5-4b}$$

Coupled-Mode Equations

where

$$\Delta\beta = \beta_1 - \beta_2 \tag{8.5-5}$$

is the phase mismatch per unit length and

$$\begin{aligned} \mathcal{C}_{21} &= \tfrac{1}{2}\left(n_2^2 - n^2\right)\frac{k_o^2}{\beta_1}\int_a^{a+d} u_1(y)\,u_2(y)\,dy, \\ \mathcal{C}_{12} &= \tfrac{1}{2}\left(n_1^2 - n^2\right)\frac{k_o^2}{\beta_2}\int_{-a-d}^{-a} u_2(y)\,u_1(y)\,dy \end{aligned} \tag{8.5-6}$$

are coupling coefficients. We see from (8.5-4) that the rate of variation of a_1 is proportional to a_2, and vice versa. The coefficient of proportionality is the product of the coupling coefficient and the phase mismatch factor $\exp(j\,\Delta\beta\,z)$.

The coupled-mode equations may be solved by multiplying both sides of (8.5-4a) by $\exp(-j\Delta\beta z)$, taking the derivative with respect to z, substituting from (8.5-4b), and solving the resultant second-order differential equation in $a_1(z)$. The result is:

$$a_1(z) = A(z)a_1(0) + B(z)a_2(0) \tag{8.5-7a}$$

$$a_2(z) = C(z)a_1(0) + D(z)a_2(0), \tag{8.5-7b}$$

where

$$A(z) = D^*(z) = \exp\left(\frac{j\,\Delta\beta\,z}{2}\right)\left(\cos\gamma z - j\frac{\Delta\beta}{2\gamma}\sin\gamma z\right) \tag{8.5-8a}$$

$$B(z) = \frac{\mathcal{C}_{21}}{j\gamma}\exp\left(j\frac{\Delta\beta\,z}{2}\right)\sin\gamma z \tag{8.5-8b}$$

$$C(z) = \frac{\mathcal{C}_{12}}{j\gamma}\exp\left(-j\frac{\Delta\beta\,z}{2}\right)\sin\gamma z \tag{8.5-8c}$$

are elements of a transmission matrix $\mathbf{T}$ that relates the output and input fields and

$$\gamma^2 = \left(\frac{\Delta\beta}{2}\right)^2 + \mathcal{C}^2, \quad \mathcal{C} = \sqrt{\mathcal{C}_{12}\mathcal{C}_{21}}\,. \tag{8.5-9}$$

If we assume that no light enters waveguide 2 so that $a_2(0) = 0$, then the optical powers $P_1(z) \propto |a_1(z)|^2$ and $P_2(z) \propto |a_2(z)|^2$ are

$$P_1(z) = P_1(0)\left[\cos^2\gamma z + \left(\frac{\Delta\beta}{2\gamma}\right)^2\sin^2\gamma z\right] \tag{8.5-10a}$$

$$P_2(z) = P_1(0)\frac{|\mathcal{C}_{21}|^2}{\gamma^2}\sin^2\gamma z. \tag{8.5-10b}$$

Thus, power is exchanged periodically between the two waveguides, as illustrated in Fig. 8.5-6(a). The period is π/γ.

When the waveguides are identical, i.e., $n_1 = n_2$, $\beta_1 = \beta_2$, and $\Delta\beta = 0$, the two guided waves are said to be phase matched. In this case, $\gamma = \mathcal{C}$, $\mathcal{C}_{12} = \mathcal{C}_{21} = \mathcal{C}$, and the transmission matrix takes the simpler form

$$\mathbf{T} = \begin{bmatrix} A(z) & B(z) \\ C(z) & D(z) \end{bmatrix} = \begin{bmatrix} \cos \mathcal{C}z & -j \sin \mathcal{C}z \\ -j \sin \mathcal{C}z & \cos \mathcal{C}z \end{bmatrix}. \tag{8.5-11}$$

Equations (8.5-10) then simplify to

$$P_1(z) = P_1(0) \cos^2 \mathcal{C}z \tag{8.5-12a}$$

$$P_2(z) = P_1(0) \sin^2 \mathcal{C}z. \tag{8.5-12b}$$

The exchange of power between the waveguides can then be complete, as illustrated in Fig. 8.5-6(b).

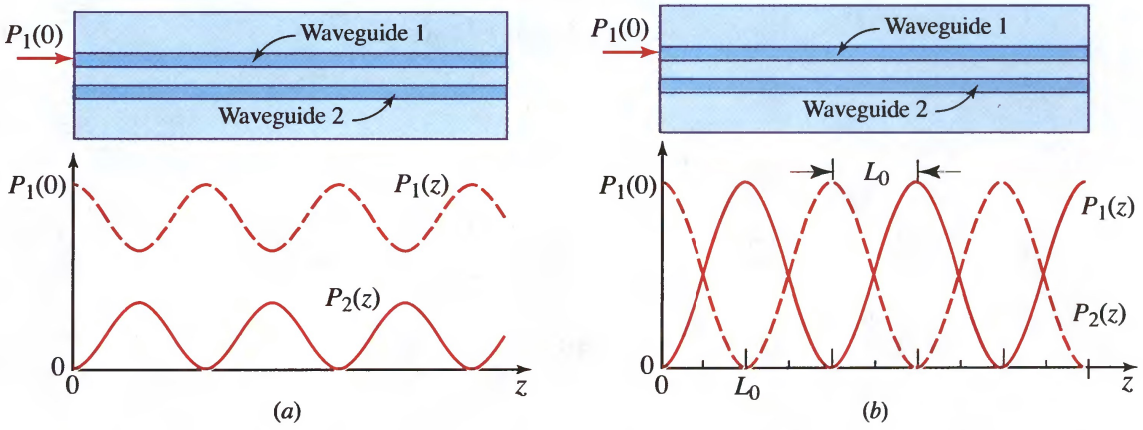

Figure 8.5-6 Periodic exchange of power between waveguides 1 and 2: (a) Phase mismatched case; (b) Phase matched case.

We thus have a device capable of coupling any desired fraction of optical power from one waveguide into another. At a distance $z = L_0 = \pi/2\mathcal{C}$, called the **coupling length** or the **transfer distance**, the power is transferred completely from waveguide 1 into waveguide 2 [Fig. 8.5-7(a)]. At a distance $L_0/2$, half the power is transferred, so that the device acts as a 3-dB coupler, i.e., a 50/50 beamsplitter [Fig. 8.5-7(b)].

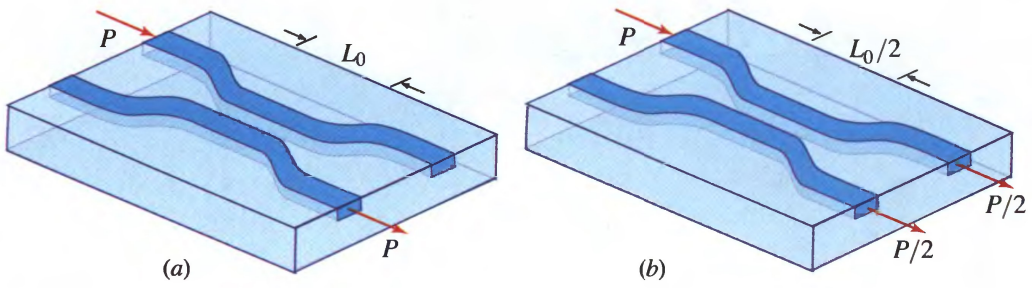

Figure 8.5-7 Optical couplers: (a) switching power from one waveguide to another; (b) a 3-dB coupler.

Switching by Control of Phase Mismatch

A waveguide coupler of fixed length, $L_0 = \pi/2\mathcal{C}$ for example, changes its power-transfer ratio if a small phase mismatch $\Delta\beta$ is introduced. Using (8.5-10b) and (8.5-9), the power-transfer ratio $\mathcal{T} = P_2(L_0)/P_1(0)$ may be written as a function of $\Delta\beta$,

$$\mathcal{T} = \frac{\pi^2}{4}\,\mathrm{sinc}^2\left[\frac{1}{2}\sqrt{1+\left(\frac{\Delta\beta\, L_0}{\pi}\right)^2}\right], \tag{8.5-13}$$

Power-Transfer Ratio

where $\mathrm{sinc}(x) = \sin(\pi x)/(\pi x)$. Figure 8.5-8 illustrates the dependence of the power-transfer ratio $\mathcal{T}$ on the mismatch parameter $\Delta\beta\, L_0$. The ratio achieves a maximum value of unity at $\Delta\beta\, L_0 = 0$, decreases with increasing $\Delta\beta\, L_0$, and then vanishes when $\Delta\beta\, L_0 = \sqrt{3}\,\pi$.

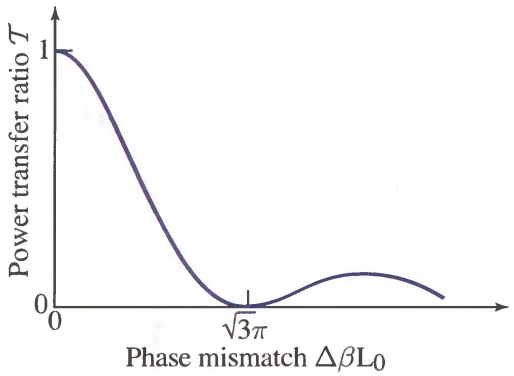

Figure 8.5-8 Dependence of the power transfer ratio $\mathcal{T} = P_2(L_0)/P_1(0)$ on the phase mismatch parameter $\Delta\beta\, L_0$. The waveguide length is chosen such that for $\Delta\beta = 0$ (the phase-matched case), maximum power is transferred to waveguide 2, i.e., $\mathcal{T} = 1$.

The dependence of the transferred power on the phase mismatch can be utilized in making electrically activated directional couplers. If the mismatch $\Delta\beta\, L_0$ is switched between 0 and $\sqrt{3}\,\pi$, the light is switched from waveguide 2 to waveguide 1. Electrical control of $\Delta\beta$ can be achieved if the material of the waveguides is electro-optic (i.e., if its refractive index can be altered by applying an electric field). Such devices will be examined in Chapters 20 and 23 in connection with electro-optic switches.

☐ ***Derivation of the Coupled Wave Equations.** We proceed to derive the differential equations (8.5-4) that govern the amplitudes $a_1(z)$ and $a_2(z)$ of the coupled modes. When the two waveguides are not interacting they carry optical fields whose complex amplitudes are of the form

$$E_1(y,z) = a_1 u_1(y)\,\exp(-j\beta_1 z) \tag{8.5-14a}$$

$$E_2(y,z) = a_2 u_2(y)\,\exp(-j\beta_2 z). \tag{8.5-14b}$$

The amplitudes a_1 and a_2 are then constant. In the presence of coupling, we assume that the amplitudes a_1 and a_2 become functions of z but the transverse functions $u_1(y)$ and $u_2(y)$, and the propagation constants β_1 and β_2, are not altered. The amplitudes a_1 and a_2 are assumed to be slowly varying functions of z in comparison with the distance β^{-1} (the inverse of the propagation constant, β_1 or β_2), which is of the order of magnitude of the wavelength of light.

The presence of waveguide 2 is regarded as a perturbation of the medium outside waveguide 1 in the form of a slab of refractive index $n_2 - n$ and width d at a distance $2a$. The excess refractive index $(n_2 - n)$ and the field E_2 correspond to an excess polarization density $P = (\epsilon_2 - \epsilon)E_2 = \epsilon_o(n_2^2 - n^2)E_2$, which creates a source of optical radiation into waveguide 1 [see (5.2-25)] $\mathcal{S}_1 = -\mu_o \partial^2 \mathcal{P}/\partial t^2$

with complex amplitude

$$S_1 = \mu_o \omega^2 P = \mu_o \omega^2 \epsilon_o \left(n_2^2 - n^2\right) E_2 = \left(n_2^2 - n^2\right) k_o^2 E_2$$
$$= \left(k_2^2 - k^2\right) E_2. \tag{8.5-15}$$

Here ϵ_2 and ϵ are the electric permittivities associated with the refractive indexes n_2 and n, respectively, and $k_2 = n_2 k_o$. This source is present only in the slab of waveguide 2.

To determine the effect of such a source on the field in waveguide 1, we write the Helmholtz equation in the presence of a source as

$$\nabla^2 E_1 + k_1^2 E_1 = -S_1 = -\left(k_2^2 - k^2\right) E_2. \tag{8.5-16a}$$

We similarly write the Helmholtz equation for the wave in waveguide 2 with a source generated as a result of the field in waveguide 1,

$$\nabla^2 E_2 + k_2^2 E_2 = -S_2 = -\left(k_1^2 - k^2\right) E_1, \tag{8.5-16b}$$

where $k_1 = n_1 k_o$. Equations (8.5-16) are two coupled partial different equations that we solve to determine E_1 and E_2. This type of perturbation analysis is valid only for weakly coupled waveguides.

We now write $E_1(y,z) = a_1(z)\, e_1(y,z)$ and $E_2(y,z) = a_2(z)\, e_2(y,z)$, where $e_1(y,z) = u_1(y)\exp(-j\beta_1 z)$ and $e_2(y,z) = u_2(y)\exp(-j\beta_2 z)$ and note that e_1 and e_2 must satisfy the Helmholtz equations,

$$\nabla^2 e_1 + k_1^2 e_1 = 0 \tag{8.5-17a}$$

$$\nabla^2 e_2 + k_2^2 e_2 = 0, \tag{8.5-17b}$$

where $k_1 = n_1 k_o$ and $k_2 = n_2 k_o$ for points inside the slabs of waveguides 1 and 2, respectively, and $k_1 = k_2 = n k_o$ elsewhere. Substituting $E_1 = a_1 e_1$ into (8.5-16a), we obtain

$$\frac{d^2 a_1}{dz^2}\, e_1 = 2\frac{da_1}{dz}\frac{de_1}{dz} = -\left(k_2^2 - k^2\right) a_2 e_2. \tag{8.5-18}$$

Noting that a_1 varies slowly, whereas e_1 varies rapidly with z, we neglect the first term of (8.5-18) in comparison with the second. The ratio between these terms is $[(d\Psi/dz)e_1]/[2\Psi de_1/dz] = [(d\Psi/dz)e_1]/[2\Psi(-j\beta_1 e_1)] = j(d\Psi/\Psi)/2\beta_1\, dz$ where $\Psi = da_1/dz$. The approximation is valid if $d\Psi/\Psi \ll \beta_1\, dz$, i.e., if the variation in $a_1(z)$ is slow in comparison with the length β_1^{-1}.

We proceed by substituting $e_1 = u_1 \exp(-j\beta_1 z)$ and $e_2 = u_2 \exp(-j\beta_2 z)$ into (8.5-18). Neglecting the first term leads to

$$2\frac{da_1}{dz}(-j\beta_1)\, u_1(y)\, e^{-j\beta_1 z} = -\left(k_2^2 - k^2\right) a_2\, u_2(y)\, e^{-j\beta_2 z}. \tag{8.5-19}$$

Multiplying both sides of (8.5-19) by $u_1(y)$, integrating with respect to y, and using the fact that $u_1^2(y)$ is normalized so that its integral is unity, we finally obtain

$$\frac{da_1}{dz}\, e^{-j\beta_1 z} = -j\mathcal{C}_{21}\, a_2(z)\, e^{-j\beta_2 z}, \tag{8.5-20}$$

where $\mathcal{C}_{21}$ is given by (8.5-6). A similar equation is obtained by repeating the procedure for waveguide 2. These equations yield the coupled differential equations (8.5-4). ■

C. Periodic Waveguides

The analysis of light propagation in two coupled parallel planar waveguides may, in principle, be generalized to multiple waveguides, although the resultant coupled equations are difficult to solve. In the limit of a large number of parallel identical slabs separated by equal distances, the theory of light propagation in periodic media, which is

presented in Sec. 7.2, may be readily applied. It is instructive to compare the dispersion diagram for light propagation in a slab dielectric waveguide, as shown in Fig. 8.2-8(a), to that for light propagation in a periodic dielectric medium comprising a collection of parallel dielectric slabs, as shown in Fig. 7.2-7. These diagrams are reproduced in Fig. 8.5-9 for comparison.

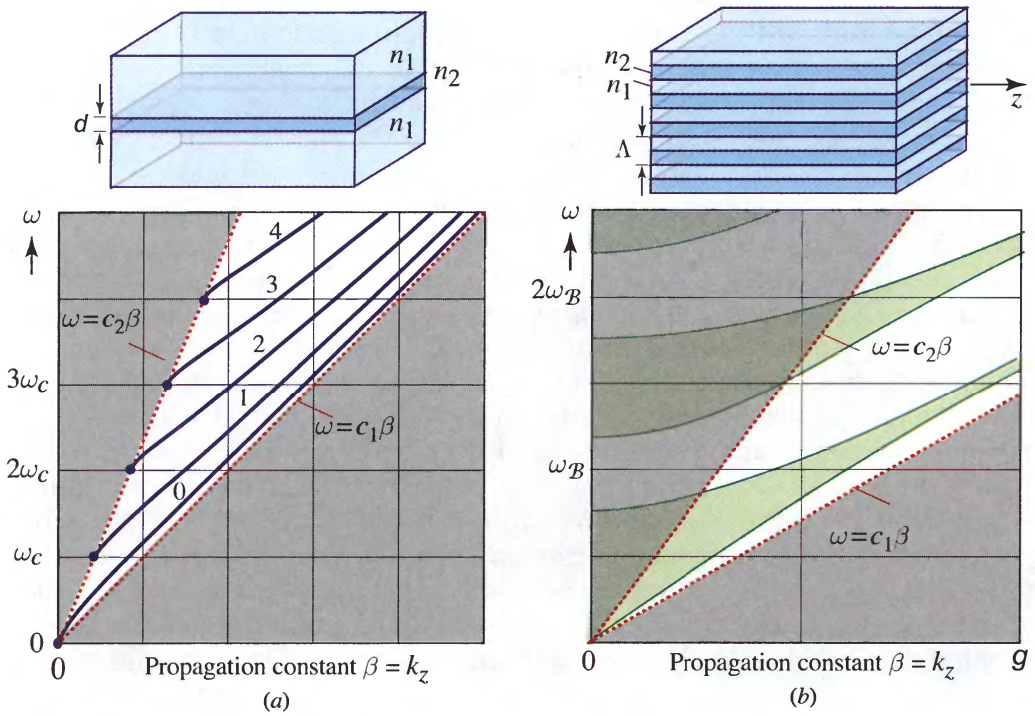

Figure 8.5-9 Dispersion diagram of (a) slab waveguide with cutoff angular frequency $\omega_c = (\pi/d)(c_o/\mathrm{NA})$; ($b$) periodic waveguide with Bragg angular frequency $\omega_{\mathcal{B}} = (\pi/\Lambda)(c_o/\bar{n})$.

In the single-slab waveguide, light travels in modes, each with a dispersion line lying in the region between the light lines $\omega = c_1\beta$ and $\omega = c_2\beta$. At any frequency, there is at least one mode. In the periodic waveguide, the dispersion lines broaden into bands separated by photonic bandgaps. Here, we assume that the modes travel in a direction parallel to the layers (the z direction in Fig. 8.5-9, which corresponds to the x direction in Fig. 7.2-7), so that the bands also lie in the region between the light lines.

8.6 SUB-WAVELENGTH METAL WAVEGUIDES (PLASMONICS)

As shown in earlier sections of this chapter, it is difficult to confine an optical wave to dimensions much smaller than a wavelength (see also Sec. 4.4D). In the mirror waveguide described in Sec. 8.1, for example, a wave of wavelength λ cannot be guided if the mirror separation d is smaller than $\lambda/2$ (since the wave frequency would then be smaller than the cutoff frequency $c/2d$). In the slab dielectric waveguide described in Sec. 8.2, if the width d is reduced below $\lambda/2$, only a single mode can be supported, and if d is reduced further, there is substantial leakage of the guided wave into the cladding. Light can, however, be confined and guided at the sub-wavelength scale by the use of sub-wavelength metallic structures, such as thin films and metallic particles buried in dielectric media. This approach has become feasible in recent years as a result of advances in nanotechnology (nanostructures and nanoparticles), and the field is known as **plasmonics**.

The propagation of light in a bulk metal was described in Sec. 5.5D. It was shown that at frequencies below the plasma frequency, the optical wave decays with an attenuation coefficient that decreases as the frequency increases, and vanishes at the plasma frequency; the free electrons then undergo longitudinal oscillations associated with **plasmons**. Clearly, bulk metals cannot confine and guide optical waves. At a metal–dielectric interface, however, Maxwell's equations admit solutions in the form of charge-density waves coupled with optical waves, generally referred to as **surface plasmon polaritons (SPPs)**. The conduction electrons oscillate in the longitudinal direction and the electromagnetic field is confined to sub-wavelength dimensions near the surface of the metal. These coupled waves can be excited at frequencies below the plasma frequency and become most localized at the plasma frequency. SPPs allow light to be controlled and manipulated at the nanometer spatial scale, while retaining the high temporal frequency associated with optical waves.

Waveguides based on SPPs can, for example, be implemented by using a dielectric slab surrounded by metallic claddings. The width of the slab must be sufficiently small for the confined SPP waves at the claddings to overlap, thereby permitting the coupled SPP waves to be guided. The dispersion relation for such a structure may be obtained by matching the boundary conditions at the dielectric–metal interfaces using, e.g., the Drude model for the metal (see Sec. 5.5D). For sufficiently small slab thicknesses, large propagation constants can be achieved even for frequencies far below the bulk-metal plasma frequency. These plasmonic waveguides are made of **metal/insulator/metal (MIM)** heterostructures of submicrometer dimensions. Modes at near-infrared wavelengths can be localized at the nanometer scale, but the propagation length is limited.

Another class of plasmonic waveguides with subwavelength mode size makes use of arrays of metallic nanoparticles that are sufficiently close so that their localized plasmonic fields overlap. Such **metamaterials** (see Sec. 5.7) admit guided modes of submicrometer size at frequencies of the individual particle plasmons or at the interparticle gap resonance.

Plasmonics seeks to couple the domains of highly integrated electronics (with dimensions < 100 nm) and optical-frequency photonics (with bandwidths > 100 THz). It is envisioned to have a number of valuable applications in **nano-optics**, including intrachip interconnects; the transmission of light through objects that are ordinarily opaque (as a result of plasmon excitations at nanosize holes in the material); the creation of distributed point sources of light generated at the surfaces of metallic-coated nanosize objects; and devices such as nanoantennas, nanoresonators, and nanowaveguides that are analogous to electrical circuit elements but operate in the visible region of the spectrum. Biosensing applications, based on the sensitivity of plasmon excitations to the properties of a dielectric medium surrounding a metallic nanostructure, include measurements of the thickness of colloidal films as well as the screening and quantifying of protein binding events.

READING LIST

Books

C.-L. Chen, *Foundations for Guided Wave Optics*, Wiley, 2006.

K. Iga and Y. Kokobun, eds., *Encyclopedic Handbook of Integrated Optics*, CRC Press, 2006.

A. Sharma, ed., *Guided Wave Optics*, Anshan, 2006.

K. Okamoto, *Fundamentals of Optical Waveguides*, Elsevier, 2nd ed. 2005.

B. P. Pal, ed., *Guided Wave Optical Components and Devices: Basics, Technology, and Applications*, Academic Press, 2005.

G. T. Reed and A. P. Knights, *Silicon Photonics*, Wiley, 2004.

G. Lifante, *Integrated Photonics: Fundamentals*, Wiley, 2003.

C. Pollock and M. Lipson, *Integrated Photonics*, Kluwer, 2003.

A. A. Barybin and V. A. Dmitriev, *Modern Electrodynamics and Coupled-Mode Theory: Application to Guided-Wave Optics*, Rinton Press, 2002.

R. G. Hunsperger, *Integrated Optics: Theory and Technology*, Springer-Verlag, 1982, 5th ed. 2002.

K. Iizuka, *Elements of Photonics, Volume 2: For Fiber and Integrated Optics*, Wiley, 2002.

R. W. Waynant and J. K. Lowell, *Electronic and Photonic Circuits and Devices*, IEEE Press, 1998.

W. B. Leigh, *Devices for Optoelectronics*, Marcel Dekker, 1996.

L. A. Coldren and S. W. Corzine, *Diode Lasers and Photonic Integrated Circuits*, Wiley, 1995.

H. P. Zappe, *Introduction to Semiconductor Integrated Optics*, Artech, 1995.

R. G. Hunsperger, ed., *Photonic Devices and Systems*, Marcel Dekker, 1994.

Y. Suematsu and A. R. Adams, eds., *Handbook of Semiconductor Lasers and Photonic Integrated Circuits*, Chapman & Hall, English ed. 1994.

O. Wada, ed., *Optoelectronic Integration: Physics, Technology, and Applications*, Kluwer, 1994.

K. J. Ebeling, *Integrated Optoelectronics: Waveguide Optics, Photonics, Semiconductors*, Springer-Verlag, 1993.

A. R. Mickelson, *Guided Wave Optics*, Springer-Verlag, 1993.

L. A. Hornak, ed., *Polymers for Lightwave and Integrated Optics: Technology and Applications*, Marcel Dekker, 1992.

J. E. Midwinter and Y. L. Guo, *Optoelectronics and Lightwave Technology*, Wiley, 1992.

R. Syms and J. Cozens, *Optical Guided Waves and Devices*, McGraw–Hill, 1992.

M. Young, *Optics and Lasers: Including Fibers and Optical Waveguides*, Springer-Verlag, 4th revised ed. 1992.

D. Marcuse, *Theory of Dielectric Optical Waveguides*, Academic Press, 1974, 2nd ed. 1991.

T. Tamir, ed., *Guided-Wave Optoelectronics*, Springer-Verlag, 2nd ed. 1990.

D. Marcuse, *Light Transmission Optics*, Van Nostrand Reinhold, 1972, 2nd ed. 1982; Krieger, reissued 1989.

H. Nishihara, M. Haruna, and T. Suhara, *Optical Integrated Circuits*, McGraw–Hill, 1989.

S. Solimeno, B. Crosignani, and P. Di Porto, *Guiding, Diffraction, and Confinement of Optical Radiation*, Academic Press, 1986.

Articles

Issue on nanophotonics, *IEEE Journal of Selected Topics in Quantum Electronics*, vol. 12, no. 6, 2006.

M. Paniccia and S. Koehl, The Silicon Solution, *IEEE Spectrum*, vol. 42, no. 10, pp. 38–43, 2005.

Issue on integrated optics and optoelectronics, Part II, *IEEE Journal of Selected Topics in Quantum Electronics*, vol. 11, no. 2, 2005.

Issue on integrated optics and optoelectronics, Part I, *IEEE Journal of Selected Topics in Quantum Electronics*, vol. 11, no. 1, 2005.

Special issue on integrated optics, *Applied Physics B: Lasers and Optics*, vol. 73, no. 5–6, 2001.

Millennium issue, *IEEE Journal of Selected Topics in Quantum Electronics*, vol. 6, no. 6, 2000.

Issue on integrated optics and optoelectronics, *IEEE Journal of Selected Topics in Quantum Electronics*, vol. 6, no. 1, 2000.

D. G. Hall, ed., *Selected Papers on Coupled Mode Theory in Guided-Wave Optics*, SPIE Optical Engineering Press (Milestone Series Volume 84), 1993.

PROBLEMS

8.1-3 **Field Distribution.**

(a) Demonstrate that a single TEM plane wave $E_x(y, z)=A\exp(-jk_y y)\exp(-j\beta z)$ cannot satisfy the boundary conditions, $E_x(\pm d/2, z) = 0$ at all z, in the mirror waveguide illustrated in Fig. 8.1-1.

(b) Show that the sum of two TEM plane waves written as $E_x(y,z) = A_1 \exp(-jk_{y1}y) \exp(-j\beta_1 z) + A_2 \exp(-jk_{y2}y) \exp(-j\beta_2 z)$ does not satisfy the boundary conditions if $A_1 = \pm A_2$, $\beta_1 = \beta_2$, and $k_{y1} = -k_{y2} = m\pi/d$ where $m = 1, 2, \ldots$.

8.1-4 **Modal Dispersion.** Light of wavelength $\lambda_o = 0.633$ μm is transmitted through a mirror waveguide of mirror separation $d = 10$ μm and $n = 1$. Determine the number of TE and TM modes. Determine the group velocities of the fastest and the slowest mode. If a narrow pulse of light is carried by all modes for a distance 1 m in the waveguide, how much does the pulse spread as a result of the differences of the group velocities?

8.2-3 **Parameters of a Dielectric Waveguide.** Light of free-space wavelength $\lambda_o = 0.87$ μm is guided by a thin planar film of width $d = 2$ μm and refractive index $n_1 = 1.6$ surrounded by a medium of refractive index $n_2 = 1.4$.

(a) Determine the critical angle θ_c and its complement $\bar{\theta}_c$, the numerical aperture NA, and the maximum acceptance angle for light originating in air ($n = 1$).

(b) Determine the number of TE modes.

(c) Determine the bounce angle θ and the group velocity v of the $m = 0$ TE mode.

8.2-4 **Effect of Cladding.** Repeat Prob. 8.2-3 if the thin film is suspended in air ($n_2 = 1$). Compare the results.

8.2-5 **Field Distribution.** The transverse distribution $u_m(y)$ of the electric-field complex amplitude of a TE mode in a slab waveguide is given by (8.2-10) and (8.2-13). Derive an expression for the ratio of the proportionality constants. Plot the distribution of the $m = 0$ TE mode for a slab waveguide with parameters $n_1 = 1.48$, $n_2 = 1.46$, $d = 0.5$ μm, and $\lambda_o = 0.85$ μm, and determine its confinement factor (percentage of power in the slab).

8.2-6 **Derivation of the Field Distributions Using Maxwell's Equations.** Assuming that the electric field in a symmetric dielectric waveguide is harmonic within the slab and exponential outside the slab and has a propagation constant β in both media, we may write $E_x(y,z) = u(y)\, e^{-j\beta z}$, where

$$u(y) = \begin{cases} A\cos(k_y y + \varphi), & -d/2 \le y \le d/2, \\ B\exp(-\gamma y), & y > d/2, \\ B\exp(\gamma y), & y < d/2. \end{cases}$$

For the Helmholtz equation to be satisfied, $k_y^2 + \beta^2 = n_1^2 k_o^2$ and $-\gamma^2 + \beta^2 = n_2^2 k_o^2$. Use Maxwell's equations to derive expressions for $H_y(y,z)$ and $H_z(y,z)$. Show that the boundary conditions are satisfied if β, γ, and k_y take the values β_m, γ_m, and k_{ym} derived in the text and verify the self-consistency condition (8.2-4).

8.2-7 **Single-Mode Waveguide.** What is the largest thickness d of a planar symmetric dielectric waveguide with refractive indexes $n_1 = 1.50$ and $n_2 = 1.46$ for which there is only one TE mode at $\lambda_o = 1.3$ μm? What is the number of modes if a waveguide with this thickness is used at $\lambda_o = 0.85$ μm instead?

8.2-8 **Mode Cutoff.** Show that the cutoff condition for TE mode $m > 0$ in a symmetric slab waveguide with $n_1 \approx n_2$ is approximately $\lambda_o^2 \approx 8 n_1 \Delta n\, d^2/m^2$, where $\Delta n = n_1 - n_2$.

8.2-9 **TM Modes.** Derive an expression for the bounce angles of the TM modes similar to (8.2-4). Use a computer to generate a plot similar to Fig. 8.2-2 for TM modes in a waveguide with $\sin\bar{\theta}_c = 0.3$ and $\lambda/2d = 0.1$. What is the number of TM modes?

8.3-1 **Modes of a Rectangular Dielectric Waveguide.** A rectangular dielectric waveguide has a square cross section of area 10^{-2} mm^2 and numerical aperture NA $= 0.1$. Use (8.3-3) to plot the number of TE modes as a function of frequency ν. Compare your results with Fig. 8.2-4.

8.4-1 **Coupling Coefficient Between Two Slabs.**

(a) Use (8.5-6) to determine the coupling coefficient between two *identical* slab waveguides of width $d = 0.5$ μm, spacing $2a = 1.0$ μm, refractive indexes $n_1 = n_2 = 1.48$, in a medium of refractive index $n = 1.46$, at $\lambda_o = 0.85$ μm. Assume that both waveguides are operating in the $m = 0$ TE mode and use the results of Prob. 8.2-5 to determine the transverse distributions.

(b) Determine the length of the waveguides so that the device acts as a 3-dB coupler.

CHAPTER

9

FIBER OPTICS

Charles Kao (born 1933) promulgated the concept of using low-loss optical fibers in practical telecommunications systems.

Philip St John Russell (born 1953) invented the photonic-crystal fiber in 1991; it has found use in many applications.